Fluorescence exclusion: a rapid, accurate and powerful method for measuring yeast cell volume

Daniel García-Ruano[1], Akanksha Jain[1], Joseph C. Ryan[1], Vasanthakrishnan Radhakrishnan Balasubramaniam[1], Larisa Venkova[2], Matthieu Piel[2] and Damien Coudreuse[1,*]

[1] Institute of Genetics and Development of Rennes, UMR 6290, CNRS – University of Rennes 1, France

[2] Institut Curie and Institut Pierre Gilles de Gennes, PSL Research University, CNRS UMR 144, Paris, France.

[*] Corresponding author: damien.coudreuse@univ-rennes1.fr

SUMMARY STATEMENT

Fluorescence exclusion provides a unique method to accurately measure the volume of yeast cells at both the population and single-cell levels.

ABSTRACT

Cells exist in an astonishing range of volumes across and within species. However, our understanding of cell size control remains limited, due in large part to the challenges associated with accurate determination of cell volume. Much of our comprehension of size regulation derives from models such as budding and fission yeast, but even for these morphologically stereotypical cells, assessment of cell volume has relied on proxies and extrapolations from two-dimensional measurements. Recently, the fluorescence exclusion method (FXm) was developed to evaluate the size of mammalian cells, but whether it could be applied to smaller cells remained unknown. Using specifically designed microfluidic chips and an improved data analysis pipeline, we show here that FXm reliably detects subtle differences in the volume of fission yeast cells, even for those with altered shapes. Moreover, it allows for the monitoring of dynamic volume changes at the single-cell level with high time resolution. Collectively, our work reveals how coupling FXm with yeast genetics will bring new insights into the complex biology of cell growth.

KEYWORDS

Cell volume, yeast, fluorescence exclusion

RUNNING TITLE

Measuring yeast cell volume

INTRODUCTION

Regulation of cell volume is central to the biology of living organisms. It is a dynamic and complex trait that is modulated by both genetic and environmental components (Amodeo and Skotheim, 2016; Cook and Tyers, 2007; Lloyd, 2013; Marshall et al., 2012; Mueller, 2015). It has an impact on a host of processes, ranging from cytoskeletal dynamics (Pedersen et al., 2001) to the scaling of global transcription rates (Zhurinsky et al., 2010). In metazoa, cell volume contributes to the overall size and shape of an organism and plays important roles in the development and architecture of tissues (Amodeo and Skotheim, 2016; Cook and Tyers, 2007; Lloyd, 2013; Marshall et al., 2012; Mueller, 2015). At the single-cell level, volume and surface area not only define how cells sense external stimuli and interact with their environment but also determine their intracellular chemistry and organization. Moreover, cell size has a profound impact on basic nuclear functions. Indeed, in a number of organisms, nuclear size scales with cell size, and the nucleo-cytoplasmic ratio was shown to be constant in a range of conditions (Jorgensen et al., 2007; Neumann and Nurse, 2007). This is poised to affect chromatin-related processes as well as events that require highly regulated nuclear mechanics such as chromosome segregation. Strikingly, deregulation of cell size has dramatic consequences and is a hallmark of aging and cancer development (Li et al., 2015; Pietras, 2011; Yang et al., 2011).

In proliferating cells, volume is intimately linked to the processes that control cell cycle progression. The dynamics of cell growth are complex across species, and specific stages of the cell cycle are associated with differential changes in cell size and morphology. For instance, while cells of the fission yeast *Schizosaccharomyces pombe* stop growing and maintain their overall shape during mitosis, mammalian cells undergoing division show a transient phase of rounding and volume alteration (Lancaster et al., 2013; Zlotek-Zlotkiewicz et al., 2015). In addition, size thresholds have been proposed to act as key checkpoints during the fission yeast cell cycle, allowing for the coordination of growth and division (Fantes, 1977; Fantes and Nurse, 1978; Fantes and Nurse, 1977). These corrective mechanisms reduce the cell-to-cell heterogeneity that can result from variability in cell size at birth or asymmetric cell division, thereby maintaining size homeostasis in a growing population. Interestingly, increases in cell volume were frequently observed during long-term experimental evolution in bacteria and were proposed to contribute to improved proliferation (Grant et al., 2021; Lenski and Travisano, 1994; Mongold and Lenski, 1996). This highlights how the volume of dividing cells may result from the necessary balance between growth advantages and evolutionary trade-offs.

Alterations in cell size are triggered by changes in the environment, such as upon modulation of nutritional conditions, and cell cycle exit is often associated with a decrease in cell volume. For example, yeast cells exposed to nitrogen or glucose starvation enter quiescence with a significantly reduced size (Sun and Gresham, 2021). However, the coupling of growth and proliferation is more complex, playing a key role in organismal structure. In adult *C. elegans* where total cell number is

constant, changes in cell volume directly impact the size of the animal (Cook and Tyers, 2007; Watanabe et al., 2007). In contrast, alteration of proliferation in *Drosophila* can be compensated by modulation of cell size (Neufeld et al., 1998; Su and O'Farrell, 1998; Weigmann et al., 1997).

The principles and mechanisms underlying the control of cell size have been the focus of in-depth investigation in a broad range of organisms. While several pathways have been described to play a role in regulating this critical parameter (Amodeo and Skotheim, 2016; Cook and Tyers, 2007; Lloyd, 2013; Marshall et al., 2012; Mueller, 2015), whether they represent the key mechanisms that ensure size homeostasis remains unclear. Furthermore, how cells measure and control their geometric characteristics is surprisingly poorly understood. As a result, multiple models that are not mutually exclusive have been proposed. According to these models, cells may divide 1) when they have reached a specific size (sizer), 2) after a specific time following a landmark cell cycle event (timer) and 3) after having produced a fixed amount of mass, at a rate that relies on birth size (adder). While all three possibilities are supported by experimental and theoretical studies (Fantes and Nurse, 1977; Mueller, 2015; Soifer et al., 2016; Sveiczer et al., 1996; Taheri-Araghi et al., 2015), general conclusions are difficult to draw. This may be due in part to the diversity of measurements used to describe cell size, including volume, surface area, cell length or dry mass. Indeed, the question remains whether one or a combination of these characteristics is more relevant for understanding size regulation and whether different cell types rely on the same or on distinct parameters. Thus, while the sizes and shapes of individual cell types are commonly accepted as fundamental hallmarks of cell identity, no unifying principles for size control have emerged.

Experimentally, the regulation of cell size has been difficult to study in multicellular eukaryotes, due to the complexity of modulating the characteristics of cells that are integrated in tissues with relatively stable local chemical and physical properties. Even in mammalian cell lines, the challenges of advanced genetic manipulation and the lack of simple methods for accurate measurement of parameters such as volume and surface area have been an obstacle to investigating the molecular mechanisms of cell size control. Therefore, unicellular eukaryotes such as the budding and fission yeasts remain the models of choice for deciphering the bases of this critical cellular feature. In these organisms, regulation of cell size is intimately linked to the operation of the cell cycle machinery. However, how this coupling operates, how cells monitor their dimensions and how variation from the target size triggers a corrective response are not fully understood. Several concepts have emerged that may provide robust ways of regulating size (Amodeo and Skotheim, 2016). For example, titration mechanisms involving a factor that scales with cell size and a constant reference may suffice for size control. Geometric parameters including cell length or surface area may also be involved. This may be particularly appropriate for cells with a stereotyped shape such as the fission yeast (Facchetti et al., 2019), but it is more complex to envisage in other situations.

122 In the fission yeast *S. pombe*, the existence of cell size checkpoints was initially suggested at both
123 S phase and, more importantly, mitosis (Fantes, 1977; Fantes and Nurse, 1978; Fantes and Nurse, 1977).
124 While an elegant geometric mechanism based on an intracellular gradient of a cell cycle regulator was
125 subsequently proposed (Martin and Berthelot-Grosjean, 2009; Moseley et al., 2009), recent evidence
126 challenged this model (Amodeo and Skotheim, 2016; Pan et al., 2014a; Saunders et al., 2012), and the
127 pathways controlling fission yeast cell size remain unclear. Moreover, the commonly-employed
128 approach of using cell length at division as a proxy for size may not be sufficient for investigating size
129 regulation. Indeed, slight changes in the diameter of these rod-shaped cells are usually ignored, although
130 they have a stronger impact on cell volume than similar alterations of cell length: considering a fission
131 yeast cell as a cylinder with half spheres at both ends, the volume of the cell 1) is linearly dependent on
132 the length of the cylinder and dependent on the square of its radius and 2) involves the cube of the radius
133 for each end. This is particularly relevant, as cell volume is a parameter that is more critical to cell
134 biology and biochemistry than 2-dimensional cell length. In addition, morphology mutants or cells
135 grown in conditions that induce alteration of cellular dimensions and scaling become complex to study
136 and to compare with reference strains. Finally, size at division restricts the analysis to only a small
137 fraction of a proliferating population.

138 To investigate the control of yeast cell volume in a more unbiased manner, different techniques
139 have been applied. These include volume calculation from geometrical assumptions, 2D imaging data
140 that allow 3D reconstruction or the integration of cellular sections extrapolated from the cell outlines,
141 and complex approaches using advanced micromechanical devices (Baybay et al., 2020; Bryan et al.,
142 2010; Bryan et al., 2014; Facchetti et al., 2019; Model, 2018; Pan et al., 2014b; Zegman et al., 2015).
143 However, these strategies are either low-throughput, difficult to establish or rely on various assumptions
144 and complex processing of 2D measurements. For instance, accurate evaluation of cell volume based
145 on automated recognition of cell outlines requires this detection to be highly precise in both wild type
146 and mutant strains (Baybay et al., 2020; Zegman et al., 2015), which is crucial given the impact of cell
147 diameter on cell volume. Therefore, while these methods represent important steps in our capacity to
148 address the regulation of cell volume, a more direct and simple methodology that does not introduce
149 the biases of 2D data acquisition and multiple steps of image segmentation and reconstruction is
150 necessary. This will allow us to precisely determine single cell volume in a large number of yeast cells
151 irrespective of cell morphology, throughout the cell cycle and in successive rounds of division.

152 The impact of cell morphology on volume measurement was recently addressed in mammalian
153 cells through the development of a fluorescence exclusion method (FXm) for evaluating cell volume
154 (Cadart et al., 2017). FXm relies on microfluidic devices in which cells are imaged in the presence of a
155 fluorescently-labelled dextran that does not cross the plasma membrane. Thus, using chambers of
156 known height, the local reduction in fluorescence due to the presence of a cell allows for the
157 determination of the volume of this cell with high accuracy (Fig. 1A). This technique is simple and only

158 requires single-plane imaging with low magnification objectives. It is entirely uncoupled from any
159 global or local morphological alterations and is compatible with the monitoring of high numbers of
160 cells. Although perfectly adapted to large mammalian cells, whether this new approach could be used
161 for smaller cells such as yeast remained unclear, as this would require microdevices with significantly
162 lower internal chambers. For example, while HeLa cells are around 20-40 µm in diameter with a volume
163 ranging from ~1500 μm^3 at birth to ~3000 μm^3 at division (Cadart et al., 2018; Cadart et al., 2019), wild
164 type fission yeast cells divide at a length of ~14 µm, with a diameter of ~4-4.5 µm. This gives an
165 approximate calculated volume at division, depending on the conditions and exact diameter, between
166 ~120 and 200 μm^3 (Navarro and Nurse, 2012; Nurse, 1975).

167 Here we use the fission yeast *Schizosaccharomyces pombe* as a model system and demonstrate that
168 the fluorescence exclusion method is a unique tool for measuring the volume of such small cells. We
169 fabricate specific microdevices for these cells, assess the reproducibility and sensitivity of the system,
170 and provide an improved way to perform large-scale analyses. Furthermore, we demonstrate the
171 compatibility of the approach with multi-color imaging for evaluating single-cell volume in specific
172 subpopulations. We then show how time-lapse experiments using these devices are a powerful strategy
173 to couple advanced yeast genetics with volume measurements for deciphering growth dynamics and
174 size modulation. Interestingly, comparing results from length *vs.* volume measurements suggests that
175 re-evaluating previous models and conclusions based on the former will be essential for understanding
176 how cell volume is regulated in this unicellular organism, with implications for the general principles
177 that govern cell size control in more complex eukaryotes.

178

179 **RESULTS**

180 **Microfluidic devices for determining the volume of yeast cells by fluorescence exclusion**

181 FXm was developed to accurately measure the volume of mammalian cells in an unbiased manner,
182 irrespective of the cell type and despite complex cell morphologies (Cadart et al., 2017; Cadart et al.,
183 2018). This method has the advantage of being simple and potentially compatible with any type of
184 microscopic object, making it an ideal approach for investigating the regulation of cell volume in
185 genetically amenable models such as yeast. However, to ensure an optimal and broad dynamic range
186 for accurate measurements, the internal height of the microfluidic chamber must be of the same order
187 of magnitude as that of the cells. Indeed, in the presence of a cell, the exclusion of fluorescent molecules
188 in a microsystem several times higher than the cell would only marginally affect the total fluorescence
189 intensity in the region of interest, impacting the reliability of the results. Microfluidic devices employed
190 to determine mammalian cell volume are therefore not adapted to small fission yeast cells, which require
191 chambers of ~ 4-7 µm in height, depending on the strain studied. Interestingly, evaluation of FXm

192 suggests that such reduced heights represent an advantage for the accuracy of these types of
193 measurements (Model, 2020).

194 This design constraint led us to build specific and optimized devices for our yeast model. When
195 made using the most common elastomer for microfabrication, PDMS (see Materials and Methods),
196 microfluidic chips of such reduced height require the integration of vertical structures to support the
197 chamber ceiling, preventing its collapse during the bonding of the chip to a glass coverslip. Cells in
198 close vicinity of these pillars must be excluded from the FXm measurements, due to the bias introduced
199 in their volume determination by the presence of a neighboring PDMS structure (Cadart et al., 2017).
200 The density of pillars, which also serve as normalization references during the image analysis (Cadart
201 et al., 2017), must therefore be sufficient to ensure chamber integrity while maintained as low as
202 possible to increase the throughput of the technique. To establish the most appropriate design for our
203 experiments, we tested chambers with inter-pillar distances of 120, 180 and 270 µm (Fig. 1B). We
204 found a distance of 180 µm between pillars coupled with an optimized cell concentration and
205 preparation procedure to be the most reliable combination for the measurement of high numbers of
206 individual cells in a single frame while preventing chamber collapse and limiting cell aggregation (Fig.
207 1C, see Materials and Methods).

208

209 **Measuring the volume of individual fission yeast cells using FXm**

210 The necessity to use microfluidic chambers of reduced height may represent a challenge for the
211 precise measurement of the volume of individual yeast cells. Indeed, in these conditions, the difference
212 between the minimum (pillar) and maximum (no cell) fluorescence intensities (Fig. 1A), as well as the
213 extent of fluorescent molecule displacement in the presence of a cell, are inherently low. This may
214 render the technique less sensitive and more susceptible to noise in fluorescence measurements, with
215 consequences for its accuracy and reproducibility.

216 In order to evaluate whether FXm provides high quality results for yeast, we measured the size of
217 wild type fission yeast cells, comparing both the median volumes and volume distributions from
218 independent experiments (see Materials and Methods). To this end, we used a 5.53 µm high chamber
219 design and analyzed five replicates performed in separate devices built from the same master mold.
220 Remarkably, we obtained highly reproducible data, with a median volume for the pooled datasets of
221 104.8 ± 24.5 μm^3 (standard error for the 5 replicates, s.e.m.: 1.7 μm^3), and comparable population
222 profiles (Fig. 2A). This value for wild type cells is consistent with previous results established by
223 complex image processing (Baybay et al., 2020), validating FXm for cell size monitoring in yeast. In
224 contrast to cell size at division, which only focuses on a small subpopulation, our method describes the
225 sizes of the cells over the entire population, from birth to division. It therefore integrates the normal
226 changes in volume that occur during the division cycle. In addition, our experiments suggest that several

227 repeats may be needed when evaluating median volume differences of less than 10 %, as such alteration
228 is in the range of the observed experimental variability (Fig. 2A). However, when considering a
229 geometric cell model consisting of a cylinder of with two half spheres at both ends and a constant cell
230 diameter of 4 µm, an increase of 10 % in cell volume at division is the result of an increase in cell length
231 at division from 14 µm to ~ 15 µm. Conversely, a similar change in cell volume at constant length is
232 brought about by an increase in cell diameter of ~ 0.2 µm. In both cases, these differences in 2D
233 parameters are at the limit or below the resolution of the strategies routinely used for measuring cell
234 length or width in *S. pombe*, respectively. This demonstrates the high sensitivity of FXm for yeast cell
235 volume measurement, even when applying a conservative threshold of 10 % volume change.

236 Next, as master molds deteriorate over time when heavily used and given that the standard
237 microfabrication procedures commonly found in cell biological laboratories make it difficult to generate
238 highly reproducible chamber heights, we set out to evaluate how changes in the dimensions of the
239 devices may impact volume determination. We therefore produced microfluidic chips of various
240 heights, ranging from 4.85 to 6.95 µm, and measured the size of wild type fission yeast cells by FXm.
241 Again, we observed remarkably similar median volumes and volume distributions between
242 measurements (Fig. 2B – median volume of the pooled datasets: 106.8 ± 24.4 μm^3; s.e.m. for the 5
243 replicates: 1.9 μm^3). This shows that data obtained from assays performed with different devices can
244 be reliably compared.

245 Finally, we further validated the approach by assessing the volumes of known fission yeast size
246 mutants as well as wild type diploid cells. In particular, we measured the size of well-described
247 temperature-sensitive cell cycle mutants: *wee1-50*^{ts} (small cells) and *cdc25-22*^{ts} (large cells) (Fantes,
248 1979; Fantes and Nurse, 1978; Nurse, 1975). As anticipated, *wee1-50*^{ts} and *cdc25-22*^{ts} cells grown at
249 the permissive temperature of 25 °C showed significantly smaller and larger volumes than wild type,
250 respectively (Fig. 2C, Fig. S1A). Note that the apparent broader distribution observed in *cdc25-22*^{ts} is
251 the result of their increased overall size, as the volume profiles of these different strains are similar
252 when the data are normalized to their respective median sizes (Fig. S1C). In the case of wild type diploid
253 cells, we found that the median population volume is 1.84-fold higher than of haploid cells (Fig. 2D,
254 Fig. S1B).

255 Altogether, these experiments demonstrate that FXm with specifically adapted microfluidic chips
256 is compatible with the analysis of yeast cell volume and produces highly reproducible results.
257 Furthermore, in contrast to measurements of cell length and width, this method does not rely on 2D
258 parameters that can be difficult to accurately determine. It will therefore allow us to identify changes in
259 cell volume that result from limited global or local alterations in cell diameter. Finally, our data also set
260 a first conservative threshold of 10 % for the estimation of differences in cell volume between cell
261 populations.

262 **Improving FXm image analysis**

263 FXm image analysis consists of three main steps (Cadart et al., 2017): normalization, cell selection
264 and volume calculation. However, as this technique requires the use of a low magnification objective,
265 the size of yeast cells and the high number of cells in a frame can make it time consuming and tedious
266 to manually select individual cells using the code established for larger mammalian cells. Interestingly,
267 during the normalization procedure, a mask is generated that separates pillars and cells from the
268 background (Cadart et al., 2017). Since the majority of objects extracted at this step corresponds to valid
269 individual cells, we took advantage of the normalization mask and developed a semi-automated Python
270 script to assist the user in cell selection (see Supplementary information). Thus, instead of manually
271 delineating the multiple regions of interest (Fig. 3A), this tool offers two distinct and intuitive strategies
272 to the user:

273 First, a manual cell selection mode can be chosen. In the context of this new code, the cells pre-
274 selected by the normalization mask are magnified and displayed (Fig. 3A), allowing the user to rapidly
275 exclude incorrect objects such as dust particles or cell aggregates. This reliable approach makes the
276 analysis of a high number of cells easier and faster.

277 Second, an automated and non-discriminatory selection can be applied. In order to exclude aberrant
278 measurements (*e.g.* large cell aggregates, abnormally small dead cells), thresholds are then
279 automatically set to remove outliers based on the standard deviation (s.d.) of the measurements in the
280 population. This is more appropriate than the use of absolute cut-offs, which may need to be adjusted
281 from strain to strain. After testing different s.d. thresholds (data not shown), we found that excluding
282 values outside of 2 s.d. (1 IQR for a normal distribution) for the first and third quartiles was optimal for
283 obtaining results similar to those established with the manual method, correctly selecting between 87
284 and 92 % of the objects in our experiments (Fig. 3B).

285 Finally, our script provides the option of separating the selected cells in different groups. This is
286 particularly useful when determining the volumes of distinct subpopulations, for instance based on
287 additional fluorescence markers (see below).

288 Collectively, the improvements brought by our analysis code facilitate FXm analysis and make it
289 more powerful, providing more options to the user for in-depth and complex studies of cell populations.
290 Interestingly, while manual selection is likely to be the most accurate approach, we show that automated
291 analysis with outlier exclusion allows a rapid assessment of high numbers of cells while remaining
292 sufficiently accurate to be used when screening the volume of several different strains.

293

294

295

296 **Small variations in cell dimensions and population heterogeneity**

297 Our initial volume measurements in wild type cells and the evaluation of the experimental
298 variability associated with the use of FXm with yeast cells suggest that 10 % changes in volume and
299 above can be reliably detected by this technique (Fig. 2).

300 To further assess the sensitivity of FXm, we first determined the volume of cells showing a
301 marginal difference in cell length at division compared to wild type. To this end, we took advantage of
302 a fission yeast strain whose proliferation relies on a minimal cell cycle control network (MCN). In this
303 background, cell proliferation is solely dependent on the oscillation of a single qualitative cyclin-
304 dependent kinase (CDK) activity between two thresholds (high for mitosis and low for S phase onset)
305 (Coudreuse and Nurse, 2010). This is achieved through the expression of a fusion protein between
306 cyclin B/Cdc13 and Cdk1/Cdc2, in the absence of all other cell cycle cyclins (Coudreuse and Nurse,
307 2010). Interestingly, while behaving similarly to wild type (Coudreuse and Nurse, 2010), MCN cells
308 show a minor increase of ~ 7 % in their length at division in our experimental conditions (15 µm for
309 wild type and 16.1 µm for MCN cells, Fig. 4A). This alteration is predicted to contribute to a similar
310 increase in volume according to the geometric model of *S. pombe* cells (see above). Unexpectedly, our
311 FXm measurements showed a median volume difference of 17 % between these strains (Fig. 4A, Fig.
312 S2; compare WT and MCN). This suggests that the change in size between wild type and MCN cells is
313 not solely the result of an increase in cell length. Importantly, it demonstrates that FXm is a promising
314 approach for investigating the regulation of yeast cell volume, providing novel and more in-depth
315 information on cell size compared to the standard measure of cell length at division.

316 Next, we focused on establishing whether FXm is able to reliably detect volume changes below
317 our initial and conservative threshold of 10 %. We started by evaluating whether increasing the number
318 of independent replicates is sufficient to render FXm compatible with the monitoring of small
319 alterations in cell size. For this, we built on the results in Fig. 2A and Fig. 2C, which indicate a difference
320 in cell volume of less than 10 % between wild type cells grown at 32 *vs*. 25 ºC. Comparison of the
321 volume profiles and median values in these conditions for 5 independent experiments showed that such
322 small differences can be robustly established (Fig. 4B and Fig. S3A). Next, we investigated whether
323 even smaller alterations in cell volume at the population level could be detected when monitoring
324 progressive changes in cell size over time. As a proof-of-concept, we used the MCN cells described
325 above, as they harbor an additional mutation in the ATP-binding pocket of the Cdc2 moiety of the
326 fusion module. This makes these cells sensitive to dose-dependent and reversible inhibition of CDK
327 activity by small non-hydrolysable ATP analogues such as 3-MBPP1 (Bishop et al., 2000; Coudreuse
328 and Nurse, 2010). This allowed us to block cells in G2 using the inhibitor, let them synchronously re-
329 enter the cell cycle upon inhibitor wash off (Fig. S3B, C) and monitor volume changes in the population
330 throughout the following G2 phase with high time resolution (Fig. 4C). Remarkably, even considering

331 the experimental variability observed at certain time points, very small increases in volume (<5%) and
332 changes in growth rates could be measured, demonstrating the high sensitivity of FXm in this context.

333 In addition to the median cell volume, another critical parameter in our understanding of cell size
334 homeostasis is the size distribution in the population. Indeed, this reflects the cell-to-cell heterogeneity
335 in cell cycle progression and the strength of the size control system operating in these cells. To date,
336 most studies evaluating this feature in fission yeast have focused on variability in cell length at division.
337 However, not only does this approach exclude the majority of the population, but our results above
338 suggest that the evaluation of cell volume distribution in the entire population may lead to different
339 conclusions. To establish whether FXm measurements are sufficiently sensitive for monitoring
340 alteration of cell size distribution, we took advantage of MCN cells in which the target residues of the
341 conserved Wee1/Cdc25 feedback loop on Cdc2 are mutated (T14A Y15F, MCN-AF) (Coudreuse and
342 Nurse, 2010). Loss of this mitotic switch was previously shown to result in an increase in cell-to-cell
343 variability in length at division (Coudreuse and Nurse, 2010), and in the non-supplemented minimal
344 medium used in our experiments, we also found that these dividing cells are slightly smaller than wild
345 type (Fig. 4A). As anticipated, we observed a broader distribution of cell volume in MCN-AF compared
346 to MCN and wild type cells (Fig. 4A, D). Interestingly, the relative changes in median volume *vs.*
347 average length at division between MCN-AF, MCN and wild type provide insights into the dimensions
348 that are altered in these strains (Fig. 4A, Table S1): while MCN-AF and MCN appear to differ only in
349 length (same ratios for volume *vs.* size at division), both strains are likely to show an increase in cell
350 diameter compared to wild type (differing ratios).

351 Altogether, these results demonstrate that FXm is easier and more sensitive than previously used
352 methods, allowing for the monitoring of small alterations in cell volume and changes in size
353 homeostasis populations of yeast cells. Coupling these data with more traditional cell length
354 measurements will shed light on how changes in cell volume are mediated and whether modulations of
355 cellular geometry occur.

356

357 **Measuring the size of cells with altered geometries and morphologies**

358 As discussed above, FXm allows for the identification of small changes in size that are either
359 difficult to accurately evaluate from cell length measurements or result from below-detection alterations
360 in cell diameter. The use of cell length as a proxy is even more problematic when studying mutants or
361 conditions where dimension scaling or cell shape is altered. In the latter, cell length at division becomes
362 generally irrelevant. Furthermore, strategies using automated cell outline detection to extrapolate cell
363 volume may not be sufficiently reliable, given the impact of minor changes in diameter on cell volume.

364 As a proof-of-concept, we determined the volumes of various strains known to show defects in
365 their morphology and shape. First, we assessed the size of strains lacking Rga2, Rga4 or Rga6, which

366 are members of the RhoGAP family. These factors are involved in the regulation of polarized growth,
367 and their loss results in changes in cell geometry (Das et al., 2007; Revilla-Guarinos et al., 2016; Soto
368 et al., 2010; Villar-Tajadura et al., 2008). When ranking these strains according to their length at
369 division, we found that Δ*rga2* cells are the longest, followed by Δ*rga6* and Δ*rga4* (Fig. 5A). Strikingly,
370 FXm measurements, which integrate changes in both morphology and geometry, led to the opposite
371 conclusion, with Δ*rga4* and Δ*rga2* cells having the largest and smallest median volumes, respectively
372 (Fig. 5B, Fig. S4). These data show that cell length measurement is not reliable as a proxy for cell size
373 when studying such mutants. They also demonstrate the advantages of FXm for establishing size
374 differences between strains and determining the influence of diverse pathways on cell volume
375 regulation.

376 Next, we used FXm to evaluate the size of cells for which length can be difficult to measure or
377 inherently inaccurate due to strong alterations in their morphology. To this end, we used bent cells
378 *(Δknk1, Δtea1)* as well as cells with significant shape defects and irregular diameters (Δ*mal3*)
379 (Beinhauer et al., 1997; Mata and Nurse, 1997; Scheffler et al., 2014) (Fig. 5C). As anticipated, while
380 cell length at division could not be determined without excluding a significant fraction of the cells,
381 volume measurement by FXm allowed us to establish the profile of cell volume in the population and
382 compare it with that of wild type rod-shaped cells. This again highlights the power of this method for
383 studying size control mechanisms, independently of cell morphology (Fig. 5D, Fig. S5). Interestingly,
384 in cells with morphological defects, both the median volume and size distribution may change (Figs.
385 S4, S5), potentially reflecting alterations of their cell cycle organization and associated growth patterns.
386 This would open the door to investigating how cell shape may delineate the complex interplay between
387 cell growth and division cycle at the single-cell level.

388 Finally, we evaluated data obtained by FXm for significantly smaller cells that have stopped
389 dividing. Upon glucose exhaustion, fission yeast cells exit the cell cycle and enter a non-proliferative
390 quiescent state, which is associated with a dramatic reduction in cell size. Given the shape of the cells
391 in these conditions (Fig. 5E), determining their length and width to extrapolate cell volume is difficult
392 and unreliable. In contrast, FXm measurements established high-quality profiles of cell volume in these
393 populations (Fig. 5F, Fig. S6). This will allow for investigating the impact of cell size on cell physiology
394 and aging in this critical cellular state.

395 Collectively, this set of experiments demonstrates the versatility of FXm, which provides an
396 unprecedented ability to measure the size of any strain, irrespective of cell morphology and
397 physiological status. Our results also suggest that previous conclusions on size control in fission yeast
398 may need to be re-evaluated using FXm.

399

400

401 **Measuring the volume of specific subpopulations**

402 All the experiments presented so far consider two aspects of cell volume: its median value and its
403 distribution in the entire population. The former provides a way of rapidly comparing different strains
404 while the latter brings insights into cell size homeostasis. However, extracting the volume of specific
405 subpopulations of interest is critical for understanding how different biological processes may interact
406 with the mechanisms underlying the regulation of cell size and the coupling of cell growth and
407 proliferation. Thus, associating FXm with the use of other intracellular fluorescent markers in yeast
408 cells would represent a particularly powerful method to take advantage of advanced yeast genetics and
409 explore the complexity of size regulation in different conditions and throughout the cell cycle. Similarly,
410 this could allow for discriminating between genetically distinct strains expressing specific markers in a
411 complex population, opening the door to exploring non-cell autonomous processes that may feed into
412 volume regulation. The only critical consideration for such experiments resides in the choice of the
413 secondary markers, whose emission spectra should not bleed into the FXm channel (FITC in our
414 experiments), as this would alter the accuracy of the volume measurements.

415 To evaluate these approaches, we set out to determine cell volume at division, using the non-
416 histone chromatin-associated protein Nhp6 coupled to the red fluorescent marker mCherry. First, we
417 validated that the presence of Nhp6::mCherry in the nucleus did not induce any significant signal in the
418 FITC channel under FXm conditions (Fig. S7A). This also showed that the slightly reduced volume of
419 these cells compared to wild type (Fig. 6A, Fig. S7B) is the result of an alteration of Nhp6 function due
420 to the mCherry tag rather than an experimental artifact from mCherry fluorescence. Using our improved
421 FXm analysis code, we segmented the population of binucleated cells (~11% of the total number of
422 cells) and determined their median volume (126.3 ± 18.2 μm^3 *vs.* 93.5 ± 21.3 μm^3 for the mononucleated
423 cells, Fig. 6B). The partial overlap between mono- and binucleated cells is consistent with the
424 interruption of growth during mitosis: cell size does not change throughout nuclear division, and growth
425 only resumes in G1. Note that the volume of binucleated cells measured in our assay is consistent with
426 previous calculations of cell volume at division (Nurse, 1975) but significantly differs from calculations
427 presented in a more recent study (Navarro and Nurse, 2012). This further demonstrates that fission yeast
428 cell size cannot be reliably and reproducibly determined using single measurements of cell length and
429 diameter. Collectively, our experiments validate the possibility of combining FXm with additional
430 markers in yeast for more complex investigation of cell size control and dynamics.

431

432 **Dynamic changes in fission yeast cell volume at the population and single-cell levels**

433 Next, we set out to assess whether FXm can be reliably used to assess dynamic changes in yeast
434 cell size. First, we tested how time course experiments coupled with FXm may allow for following
435 alterations in cell volume over time in asynchronous populations. Indeed, a wide range of growth

436 conditions have been shown to strongly influence size (*e.g.* heat stress (Vjestica et al., 2013), osmotic
437 stress (Millar et al., 1995), change in nutrient availability (Fantes and Nurse, 1977; Petersen, 2009)). In
438 addition, experimentally induced modulation of cellular pathways using conditional mutants, chemical
439 genetics, or inducible/repressible promoters may result in cell size changes, and understanding these
440 dynamics may be key to determining the implication of these processes in cell size homeostasis. To
441 evaluate the use of FXm for these approaches, we took advantage of the sensitivity of MCN cells to the
442 3-MBPP1 ATP analogue. Indeed, reducing Cdc2/CDK activity in fission yeast using this method leads
443 to an increase in cell size (Chen et al., 2016; Coudreuse and Nurse, 2010). We therefore measured cell
444 volume in asynchronous MCN cells at 40-minute intervals (~1/4 of the cell cycle) after treatment with
445 0.05 µM of the 3-MBPP1 analog (Fig. 7). Our data show that MCN cells progressively increase their
446 volume, up to 1.7-fold after one doubling time. Strikingly, analysis of the changes in cell length at
447 division and volume throughout the experiment (comparison of the volume *vs.* size at division ratios,
448 Table S1) suggests complex dynamics in the respective modulations of length and diameter upon
449 inhibition of CDK activity. This demonstrates that FXm 1) can be used to easily follow short-term
450 alterations in median yeast cell size and size distribution in a population of asynchronous cells and 2)
451 provides new perspectives in our understanding of how the geometrical dimensions of these cells
452 contribute to overall cell volume.

453 The experiments above only analyze population snapshots at different time points and do not
454 monitor changes in cell size over time at the single-cell level. This type of strategy is therefore
455 incompatible with evaluating immediate responses to environmental perturbations and determining the
456 behaviors of separate cell lineages. In addition, it does not allow for relating volume at birth, growth
457 rate and volume at division within single cells. Following cell length in an entire population during
458 time-lapse experiments is tedious and introduces the same bias as discussed earlier. We therefore tested
459 whether FXm provides high quality data when performing time-lapse experiments with yeast cells.
460 First, we evaluated the experimental noise for single cells in our chips by comparing 20 successive
461 measurements of 10 individual cells over a period of ~6 seconds (Fig. 8A). Making the assumption that
462 no volume changes occur in such a short time, this showed that the experimental noise inherent to the
463 method when using chips of reduced height remains very limited. Interestingly, it also suggests that
464 when monitoring single cells, volume alterations as low as ~3% can be detected. Next, to perform time-
465 lapse experiments of several hours, we began by using modified chips in which the cell injection inlets
466 were made bigger (from 2.5 to 4 mm), acting as nutritional reservoirs to maintain growth conditions as
467 stable as possible. As fission yeast cells are non-adherent, this also required pre-coating of the chip
468 coverslip with lectin. In this context, we observed a linear increase in cell volume during each cell cycle
469 and a plateau in size around the time of cell division, corresponding to the well-described growth arrest
470 at mitosis (Mitchison, 1957; Mitchison and Nurse, 1985) (Fig. 8B). We also found that in these
471 experiments, cells divide at smaller sizes in succeeding cell cycles, suggesting that the built-in reservoirs

472 are insufficient to ensure a favorable growth environment throughout our assay. We therefore applied
473 a constant flow of fresh medium containing FITC-Dextran (~3-5 $\mu L.min^{-1}$) for the entire duration of the
474 experiments. Remarkably, in this setup, we did not detect any consistent reduction in cell volume at
475 division after each cycle (Fig. 8C). Furthermore, in the presence of flow, the growth rate (see Materials
476 and Methods) was significantly higher than without medium renewal (Fig. 8B, C). This demonstrates
477 that FXm is a unique tool for monitoring volume dynamics of small cells with a high time resolution
478 and for detecting changes in growth rate at the single-cell level. Coupled with additional markers (see
479 previous section), this technique offers an unprecedented entry into the investigation of cell size control
480 and its interplay with complex biological processes.

481

482 **DISCUSSION**

483 Regulation of cell volume is critical for eukaryotic organisms, but the mechanisms underlying this
484 process are still unclear. Yeast models have played a pioneering role in deciphering this complex trait
485 and remain at the forefront of this very active research field. However, the difficulty of accurately
486 measuring cell volume at both the population and single-cell levels in these small unicellular organisms
487 represents an obstacle for our understanding of size control and homeostasis. In fact, most studies in
488 yeast have relied on approaches that are inherently biased, as they are based on indirect proxies or 2D
489 measurements of cell dimensions and extrapolation of cell volume. Unravelling the complexity of this
490 essential cellular feature thus requires direct and more reliable methods to probe cell volume in these
491 genetically amenable models.

492 Here we show that the fluorescence exclusion method (FXm), which was initially developed for
493 ascertaining the size of larger mammalian cells, is ideal for evaluating the size of small yeast cells in
494 diverse contexts. We show that it provides high quality data on the volume profiles of yeast populations
495 irrespective of cell morphology and physiological state, allows for single-cell analysis of volume
496 changes with high time resolution and is compatible with complex studies when coupled with additional
497 fluorescent markers. Our experiments in fission yeast also demonstrate that in contrast to the
498 measurement of cell length at division, a commonly-used proxy for cell size in this organism, FXm
499 gives researchers unique access to in-depth analyses of yeast cell volume dynamics and their coupling
500 with cell cycle progression, integrating the size of cells at all stages of their division cycle. Remarkably,
501 combining FXm with time-lapse imaging provides an unprecedented tool to explore the changes in
502 growth rate and cellular geometry that occur not only during proliferation or upon major transitions
503 such as quiescence entry and exit, but also when cells respond to acute alteration in the environment.
504 Thus, provided the ease of FXm implementation and the improved software that we have developed,
505 we believe that this technique will become a new standard for investigating cell size control in yeast,
506 with implications for our knowledge of size regulation in complex eukaryotes.

507 Interestingly, our work in fission yeast led to a number of observations that may question existing
508 models of cell size regulation. First, research on *S. pombe* size control and its interplay with cell cycle
509 progression has mostly been based on two key assumptions: the diameter of proliferating haploid fission
510 yeast cells is 1) constant from one cell to another and 2) homogenous along the growing axis of the
511 cells. Thus, despite the critical impact of cell diameter on cell volume, most studies generally ignore
512 this parameter. Strikingly, our results clearly show that these assumptions can lead to incorrect
513 conclusions when comparing strains, as shown using various mutants (Figs. 4, 5). In this context, FXm
514 has the unparalleled advantage of being a direct method for volume measurement that does not rely on
515 any pre-conceived idea of cell geometry. The combination of FXm with the measurement of cell length
516 also offers an additional level of understanding of cell size dynamics in different strains and conditions.
517 Indeed, assessing the changes in volume *vs*. length in distinctive strains or upon specific perturbations
518 gives a new entry into the complexity of the regulation of cellular dimensions. For example, our data
519 suggest that when cells are arrested in their division cycle through CDK inhibition, the geometric
520 changes that occur over time are surprisingly complex, with length and volume alterations showing
521 different kinetics (Table S1, MCN + 3-MBPP1). The controls of cell length and diameter may therefore
522 operate independently in these conditions. Similarly, we find that simplifying the architecture of cell
523 cycle control or growing cell in different environments has unanticipated impacts on cell geometry,
524 affecting not only cell length but also cell diameter (Table S1).

525 Focusing on subpopulations, as is the case when using cell length at division as a proxy for cell
526 size, may also hinder our comprehension of important processes linking cell growth, morphology and
527 proliferation. For instance, our analyses of morphology mutants and the apparent changes in size
528 distribution at the population level suggest that the interplay between growth rate and the phases of the
529 cell cycle may be altered in these cells, again shedding light on potentially novel inputs and mechanisms
530 that modulate cell size dynamics. In this context, comparing the volume *vs*. cell length at division ratios
531 between distinctive *rga* mutants and wild type cells (Table S1) also indicates different cell geometries
532 in these backgrounds that may represent a promising tool to decipher the key parameters used by the
533 cells to "monitor" their size.

534 Finally, the use of natural isolates of yeast cells has become more and more widespread for
535 investigating various biological processes, and in fission yeast, these strains are well-known to be less
536 homogenous in morphology and overall size (Jeffares et al., 2015). These characteristics are largely
537 incompatible with traditional methods for volume estimation. FXm may therefore represent a unique
538 solution to fully exploit this promising resource and take advantage of advanced population genetics
539 and quantitative trait loci strategies to decipher the regulation of cell size.

540 Altogether, our work demonstrates that previous models that describe the way cell size is regulated
541 in fission yeast need to be revisited using FXm. Coupled to the wealth of knowledge on size control in
542 this organism, this approach will provide unique insights into the processes that underlie the biology of

543 cell growth. While we use fission yeast as a proof-of-concept model, our results also show that FXm
544 can be applied to any type of cells over a broad range of sizes. Our studies therefore establish the
545 versatility and power of FXm for investigating cell volume homeostasis and its regulation in small cells
546 and model organisms, contributing to our general understanding of the modulation of cellular
547 dimensions and scaling in eukaryotes.

548

549 **MATERIALS AND METHODS**

550 **Fission yeast strains and methods**

551 Standard methods and media were used (Hayles and Nurse, 1992; Moreno et al., 1991). All the strains
552 described in this study are detailed in Table S2. The deletions of *rga2*, *rga4*, *rga6*, *mal3*, *knk1* and *tea1*
553 have already been described (Soto et al., 2010; Villar-Tajadura et al., 2008) (Beinhauer et al., 1997;
554 Mata and Nurse, 1997; Revilla-Guarinos et al., 2016; Scheffler et al., 2014). All experiments were
555 carried out in non-supplemented minimal medium (EMM) at 32 ºC, except otherwise noted. To inhibit
556 CDK activity in analog-sensitive MCN strains, the 3-MBPP1 inhibitor (A602960, Toronto Research
557 Chemicals, Inc.) was dissolved in DMSO at stock concentrations of 10 or 0.4 mM and added to liquid
558 cultures at a final concentration of 1 or 0.05 µM. The percentage of binucleated cells (Fig. S3C) was
559 determined from heat fixed samples on microscope slides (70 ºC for 5 min) stained with a 11:1 solution
560 of Blankophor (1 mg/mL): DAPI (1 µg/mL).

561

562 **Microfabrication of FXm chips**

563 PDMS microfluidic chips for FXm were prepared following standard microfabrication protocols
564 (McDonald and Whitesides, 2002). In brief, master molds were made by spin-coating SU-8 2005 resin
565 (MicroChem Corp., USA) on silicon wafers using a spincoater (Laurell Technologies, USA) according
566 to manufacturer's instructions. Microstructures were then generated using high-resolution chrome
567 masks (JD phototools, UK) and 365nm UV exposure (UV KUB 3, Kloe, France) followed by PGMEA
568 (Sigma-Aldrich) development. For each mold, the height of the structures was determined as the
569 average of three measurements perpendicular to the long axis of the design (Fig. 1B) using a Veeco
570 Wyko NT9100 optical profilometer (Veeco Instruments Inc., USA). Note that molds showing
571 significant variability between the three height measurements should be either discarded or used
572 considering local rather than global averaged height. To produce chips for FXm, a 10:1 mixture of
573 PDMS (Sylgard 184, Dow Corning, USA) was cast on the SU-8 master mold and allowed to cure at 70
574 °C for 2 hours. Inlets were then made using 2.5 or 4 mm biopsy punches, and chips were bonded to
575 microscopy-grade coverslips by plasma activation (Harrick Plasma, USA).

576

577

578

579 **Preparation of fission yeast cells for FXm**

580 To perform FXm experiments, exponentially growing fission yeast cells were sampled at an optical
581 density between 0.25 and 0.45 OD_{595}. To limit the formation of cell aggregates, a mild sonication cycle
582 of 5 s at 10 % amplitude (Branson 450 Digital Sonifier, Emerson Electric Co.) was applied. This
583 treatment had no effect on the results we obtained by FXm (data not shown). In order to optimize the
584 number of cells that can be measured on a single FXm image in our chip design, cells were concentrated
585 to ~ 5.5 x 10^7 cells/mL in their own conditioned minimal medium (note that to prevent bias in our
586 volume measurements, we did not use autofluorescent rich medium). FITC-Dextran was then added to
587 the sample (FD10S, Sigma Aldrich) at a final concentration of 1 mg/mL, and cells were loaded into the
588 chip shortly before image acquisition. For evaluating the volume of quiescent cells, cells were sampled
589 24 hours after they reached 0.4 OD_{595}.

590

591 **Microscopy**

592 All microscopy experiments were carried out using an inverted Zeiss Axio Observer (Carl Zeiss
593 Microscopy LLC) equipped with a Lumencor Spectra X illumination system and an Orca Flash 4.0V2
594 sCMOS camera (Hamamatsu Photonics). Acquisition was performed using the VisiView software
595 (Visitron Systems GmbH). A Plan-Apochromat 63X/1.4 NA immersion lens and a Plan-Apochromat
596 20X/0.8 NA Ph2 lens (Carl Zeiss Microscopy LLC) were used for cell length measurements and FXm,
597 respectively. For routine volume measurements, the acquisition parameters were 100 ms exposure at 20
598 % illumination power, and 30 to 40 images were taken across the whole chambers to limit potential bias
599 due to local changes in chamber height. For the time-lapse experiments in Fig 8, 100 ms exposure at 10
600 % illumination power was used.

601

602 **Image analysis**

603 Cell length at division was determined from Blankophor images (1 mg/mL Blankophor solution,
604 A108741, Ambeed Inc.) using FIJI (National Institutes of Health) and the Pointpicker plug-in. For the
605 blankophor images in Figs. 2, 4, 5, 6 and 7, the brightness and contrast were adjusted for display
606 purposes. For routine volume measurements, images were first normalized using a custom Matlab
607 software (Cadart et al., 2017). Cell selection and volume calculation were subsequently performed using
608 the normalization mask with a new, specifically-developed Python interface (see Results). For all
609 Figures, cell selection was done using the manual mode, except for Fig. 3B and 4C where automated
610 cell identification was used. Note that except for the time-lapses in Fig. 8B and C, we systematically
611 excluded cells that were undergoing cytokinesis but that had not fully separated into two individual
612 daughter cells; this is similar to studies of cell length at division. While this category can be integrated
613 as newly-born pairs of cells using the original Matlab software (Cadart et al., 2017), manually
614 delineating the division site would introduce measurement errors. Finally, our Python code is not
615 adapted to tracking the volume of individual cells in long time-lapse experiments (Fig. 8B, C), as slight

616 cell movements make it difficult to reliably follow single cells over time when using the normalization
617 mask pre-selection. For these assays, we used the original Matlab software (Cadart et al., 2017).
618
619 **FXm time-lapse and analysis using fission yeast**
620 As fission yeast cells are non-adherent, FXm time-lapses required coverslips to be coated in order to
621 prevent cells from moving inside the chamber, which would hamper data acquisition and analysis. To
622 this end, 10 µl of 1mg/ml filtered lectin was spread in a rectangle of ~10 x 5mm at the center of the
623 coverslip and allowed to dry at 37 ºC. The coverslip was then washed once with filtered ultra-pure water
624 and dried at 37 ºC. For experiments without medium flow (Fig. 8B), Ø 4 mm inlets were made in the
625 PDMS chip using the appropriate biopsy punch. 5 µl of cells prepared as described above were loaded
626 in one inlet, and both inlets were then filled with 45 µl EMM containing the FITC-Dextran dye. Cells
627 were allowed to flow into the chamber prior to imaging. For time-lapse experiments using medium flow
628 (Fig. 8C), two successive layers of lectin were applied as above and inlets of Ø 0.75 mm were fabricated.
629 Cells were then loaded by depositing a drop of cells prepared as above over one of the inlets, and a mild
630 vacuum was applied at the other inlet using the tip of a 10 mL pipet connected to a vacuum pump. The
631 loaded chip was then connected to a flow control system (pressure generator and flow controller,
632 Elvesys, France), and a flow of medium (~ 3-5 µL/ min) containing the FITC-Dextran dye was used
633 throughout the experiment. For the analysis of the time-lapse experiments, the two daughter cells after
634 a division were manually delineated during the analysis and only one of them was followed for further
635 investigation (Fig. 8B, C). The growth rate of each individual cell was determined by calculating the
636 slopes of the traces during each cycle. This was obtained by linear regression considering the volume
637 at birth as the first time point (when an invagination is detected) and excluding the mitotic plateau: entry
638 into mitosis was assigned to the last point prior to strong reduction of growth (when two consecutive
639 points on the graph decrease the slope).
640
641
642 **ACKNOWLEDGMENTS**
643
644 We thank Pei-Yun Jenny Wu and Snezhana Oliferenko for critically reading the manuscript. We thank
645 Pascal Hersen and Giacomo Gropplero for the measurements of our chamber heights. We are grateful
646 to Paul Nurse, Snezhana Oliferenko, Pilar Perez and Phong Tran for sharing strains and reagents.
647
648
649 **COMPETING INTERESTS**
650
651 No competing interests declared.
652

FUNDING

This work was supported by a grant to DC from the Agence Nationale de la Recherche (ANR, project eVOLve, ANR-18-CE13-0009; funding for AJ and DGR) and the Région Bretagne (ARED Pombevol, funding for DGR). JCR was supported by a fellowship from the Ministère de l'Enseignement Supérieur et de la Recherche. VRB was supported by an ERC Starting Grant to DC (SyntheCycle, Grant Agreement no. 310849).

FIGURE LEGENDS

Figure 1. Microfluidic chips for FXm. A. Schematic of the principles of FXm (Cadart et al., 2017). Left panel: cells are injected in a microfluidic chip designed for FXm (see *B*) in the presence of FITC-Dextran. Pillars are integrated in the chip for ceiling support and image normalization. A low-magnification objective (20X) is used to acquire single-plane images (see *C*). Right panel: After normalization, the volume of the cell can be determined from the loss of fluorescence intensity (grey area) in the region analyzed (the precise internal height of the microfluidic chip must be determined (Cadart et al., 2017)). **B.** Schematic of the chamber design used for fission yeast cells. Left panel: design and dimensions (schematic not to scale). Right panel: all pillars used are 60 µm in diameter and separated from other pillars by 180 µm. **C.** Image of fission yeast cells injected in the presence of FITC-Dextran in the chip (prior to image normalization) in the conditions used for all our experiments.

Figure 2. Measuring the volume of fission yeast cells by FXm. *A-D*, graphs are histograms with box and whiskers plots (indicating the min, Q1, Q3 and max, with outliers determined by 1.5 IQR (interquartile range). White dot indicates the median volume). The median volume values with standard deviations are shown. **A.** Reproducibility of volume measurements of fission yeast cells by FXm. Measurements of wild type cells in five independent experiments (grey) and the total pooled dataset (black) are shown (chamber height: 5.53 µm; $n \geq 316$ for each replicate, $n=2266$ for the total dataset; values outside of the plot range (n^*) were excluded: $n^* \leq 1$ for each replicate). **B.** Impact of chamber height on the reproducibility of FXm. Measurements of wild type cells from a single culture using five distinct devices of the indicated heights (grey) and the total pooled dataset (black) are shown ($n \geq 225$ for each replicate, $n=1777$ for the total dataset; no values were outside of the plot range ($n^*=0$ for each replicate). **C.** Top panel: volume measurement by FXm using known cell size mutants. Wild type (WT), *wee1-50*^{ts} and *cdc25-22*^{ts} temperature-sensitive strains were grown exponentially at the permissive temperature of 25 °C and their volumes were evaluated by FXm. Pooled datasets ($n \geq 1144$) of three independent experiments ($n \geq 337$ for each replicate –Fig. S1A) are shown. Values outside of the plot range were excluded ($n^* \leq 6$ for each replicate). Bottom panel: blankophor images with cell length at

689 division of the corresponding strains (averages with standard deviations for pooled datasets of three
690 independent experiments, $n \geq 100$ for each replicate). Scale bars = 10 µm. At 25 °C, WT cells have a
691 reduced volume and cell length at division compared to 32 °C (see *A*, *B* and Figs. 4-7). **D.** Top panel:
692 comparison of the volume distributions in populations of wild type haploid and diploid fission yeast
693 cells as determined by FXm. Cells were grown in supplemented EMM6S at 32 °C. Pooled datasets
694 ($n \geq 1073$) for three independent experiments ($n \geq 207$ for each replicate –Fig. S1B) are shown. Values
695 outside of the plot range were excluded ($n^* \leq 1$ for each replicate). Bottom panel: blankophor images
696 with cell length at division of the corresponding strains (averages with standard deviations for pooled
697 datasets of three independent experiments, $n \geq 100$ for each replicate). Scale bars = 10 µm. In EMM6S,
698 WT cells have a volume that is similar to that in EMM (compare with *A*, *B* and Figs. 4-7) but a reduced
699 cell length at division (compare with Fig. 4A, 5A and 7), suggesting a difference in cell width between
700 these conditions.

701

702 **Figure 3. Analysis pipeline for FXm data. A.** Top panel: representative image showing the selection
703 of individual cells (multiple individual regions of interest are indicated) using the original FXm analysis
704 code. Each cell must be visually identified from the FITC image (see Fig. 1C for full frame image; the
705 area displayed here has been magnified for display purposes) and manually selected. Bottom panel:
706 representative image showing the tool that we developed, taking advantage of the image normalization
707 mask for facilitating cell selection. All objects from the FITC image are automatically identified and
708 displayed to the user at a higher magnification. Cell aggregates (bottom left), recently divided cells
709 (bottom right) or artifacts can then be rapidly and reliably excluded from the analysis by the user (red-
710 barred). **B.** Comparison of the results obtained by FXm using manual (black) and automated (grey, 2
711 s.d. filter) cell selection. Data for manual selection are from Fig. 2C. For the automated selection, 1) the
712 same images as for the manual method were used, pooling the data from all replicates, and 2) a filter
713 was applied that excludes entries that are 2 standard deviations above and below Q3 and Q1 (n^{**}),
714 respectively (unfiltered selected objects: $n \geq 1390$, excluded objects $n^{**} \leq 200$). The overlap between the
715 two approaches for both correctly assigned cells and outliers is between 87 and 92 %. Graphs are as in
716 Fig. 2.

717

718 **Figure 4. FXm allows for the detection of subtle changes in cell volume and size distribution. A.**
719 Top panel: volume measurement of wild type (WT), MCN and MCN-AF cells by FXm. Pooled datasets
720 ($n \geq 913$) of three independent experiments ($n \geq 172$ for each replicate –Fig. S2) are shown. Values outside
721 of the plot range were excluded ($n^* \leq 1$ for each replicate). Graphs are as in Fig. 2. Bottom panel:
722 blankophor images with cell length at division of the corresponding strains (averages with standard
723 deviations for pooled datasets of three independent experiments, $n \geq 100$ for each replicate). Scale bars

724 = 10 µm. **B.** Comparison of the median volumes for 5 independent replicates of wild type cells at 25
725 and 32 °C. The full datasets are presented in Fig. S3A. For each condition, the values are sorted in
726 descending order. Difference in median cell volume: 8.8 %. **C**. MCN cells grown in EMM6S at 32 °C
727 were G2-arrested using 1 µM 3-MBPP1 for 160 min and allowed to synchronously re-enter the cell
728 cycle by washing off the inhibitor (Coudreuse and Nurse, 2010) (Fig. S3B). Cells were then injected in
729 a microfluidic chip, and FXm images were acquired at 5 min intervals throughout the next G2, after
730 cells had undergone a first round of mitosis and cell division (60 min, Fig. S3C). Top panel: median
731 population volumes at the indicated time points (black line – automated cell selection) with IQR (grey
732 area) are shown. Note that the higher starting volume for MCN cells compared to other Figures results
733 from the initial G2 block, during which cells grow without dividing. The phases of the cell cycle during
734 which cell volume was measured (first G2 and mitosis/M after release –Fig. S3C) are indicated. G2
735 growth rate: 0.59 $\mu m^3.min^{-1}$ (linear regression from 60 to 110 min, prior to the mitotic plateau). From
736 125 to 140 min, the automated cell selection does not separate cells that are newly divided (17.4%,
737 25.9% and 25.5% of the selected objects at 130, 135 and 140 min, respectively, are pairs of cells; the
738 remainder of the cells have not undergone cytokinesis at these time points), resulting in an apparent
739 increased growth rate. Note the slight delay in cell cycle progression in this experiment compared to
740 Fig. S3C, which may be due to the temporary temperature downshift when cells are injected in the
741 microfluidic chip and the growth conditions when no medium flow is applied (see Fig. 8B). For each
742 time point, $214 \leq n \leq 278$ (unfiltered automatically selected objects). Outliers were removed from the
743 automatic analysis using the 2 s.d. filter (see Fig. 3B; $28 \leq n^{**} \leq 49$, representing a maximum of 18% of
744 the number of selected objects). Bottom panel: representative images for cells in the FXm chips at 85
745 min (G2), 120 min (M) and 135 min (pairs of sister cells are not excluded by the automated analysis
746 and represent a significant subset of the population at this time point, see above). **D.** Volume distribution
747 for the indicated strains as a percentage of the median volume of the population. Data are as in *A*. Values
748 outside of the plot range were excluded ($n^* \leq 10$).

749

750 **Figure 5. Measuring the volume of yeast cells with altered morphologies. A, C, E.** Blankophor
751 images with cell length at division of the indicated strains (averages with standard deviations for pooled
752 datasets of three independent experiments, $n \geq 100$ for each replicate). n.d.: not determined. Scale bars =
753 10 µm. **B.** Volume measurement by FXm of the strains in *A*. Pooled datasets ($n \geq 832$) of three
754 independent experiments ($n \geq 268$ for each replicate – Fig. S4) are shown. Values outside of the plot
755 range were excluded ($n^* \leq 1$ for each replicate). **D.** Volume measurement by FXm of the strains in *C*.
756 Pooled datasets ($n \geq 940$) of three independent experiments ($n \geq 230$ for each replicate – Fig. S5) are
757 shown. No values were outside of the plot range ($n^* = 0$ for each replicate). Data for wild type (WT) are
758 as in Fig. 2D (haploids). **E.** Blankophor images of wild type cells in exponential growth and quiescence.
759 For quiescent cells, samples were taken 24 h after the culture reached an OD_{595} of 0.4. For proliferating

760 cells, cell length at division is shown (average with standard deviation for pooled dataset of three
761 independent experiments, $n \geq 100$ for each replicate). n.d.: not determined. Scale bars = 10 µm. **F.**
762 Volume measurement by FXm of the cells in *E*. Pooled datasets ($n \geq 965$) of three independent
763 experiments ($n \geq 238$ for each replicate – Fig. S6) are shown. No values were outside of the plot range
764 ($n^*=0$ for each replicate). *C*, *D*: Experiments were carried out in EMM6S due to the presence of
765 auxotrophies in some of the mutant strains (see Table S2). *B, D, F:* Graphs are as in Fig. 2.

766

767 **Figure 6. FXm is compatible with the use of fluorescent markers to study subpopulations. A.** Top
768 panel: volume measurement of wild type (WT) and cells expressing *nhp6::mCherry* by FXm. Pooled
769 datasets ($n \geq 1568$) of three independent experiments ($n \geq 499$ for each replicate –Fig. S7B) are shown.
770 No values were outside of the plot range ($n^*=0$ for each replicate). The median volume values with
771 standard deviations are shown. Bottom panel: blankophor images with cell length at division of the
772 strains above (averages with standard deviations for pooled datasets of three independent experiments,
773 $n \geq 110$ for each replicate). Scale bars = 10 µm. **B.** Volume comparison between mono- (grey) and bi-
774 nucleated (black) cells in the population of *nhp6::mCherry* cells as in *A*. The percentages and median
775 volumes for the mono- ($n=1619$) and binucleated ($n=196$) subpopulations are indicated below the graph.
776 Binucleated cells include both septated (dashed line) and non-septated cells. *A*, *B*: Graphs are as in Fig.
777 2.

778

779 **Figure 7. Dynamic changes in cell volume at the population level.** Left panel: FXm volume
780 measurement of MCN cells after treatment with 0.05 µM of the ATP analog 3-MBPP1. Untreated wild
781 type cells (WT) were used as a control. For MCN, samples were collected and analyzed every 40 min.
782 after addition of the inhibitor ($n \geq 265$ at each time point. $n=528$ for WT). Values outside of the plot
783 range were excluded ($n^* \leq 2$ for each dataset). Graphs are as in Fig. 2. Note that the mild potential
784 bimodal distribution observed in this experiment may not be relevant, as it can also be observed in WT
785 cells but does not appear to be systematically present (Fig. 2A, B). Right panel: blankophor images with
786 average cell length at division and standard deviation for the experiment in *A*. $n \geq 100$ for WT and MCN
787 (0, 120 and 160 min). For the 40 and 80 min time points, the initial delay of mitosis due to the inhibitor
788 treatment leads to a reduction in the number of dividing cells, making it difficult to obtain similar
789 numbers for the calculation of cell length at division ($n=45$ and 22, respectively). Septation indices:
790 WT: 11.5 %, MCN 0 min: 20.4 %, MCN 40 min: 1 %, MCN 80 min: 2 %, MCN 120 min: 15.5 %,
791 MCN 160 min: 26.9 %; $n \geq 400$ for each time point. Scale bars = 10 µm.

792

793 **Figure 8. Determination and real-time monitoring of single-cell volume by FXm. A.** Evaluation of
794 FXm experimental noise using the chips designed for yeast cells. 20 consecutive images were acquired

795 in the standard FXm setup (see Materials and Methods; 100 ms exposure per image for a total
796 acquisition time of 6 s due to shutter delay) and the volumes of 10 individual cells were followed
797 throughout the experiment. This assay makes the assumption that no significant volume changes occur
798 during this 6 s time window (the generation time of wild-type fission yeast cells in these growth
799 conditions is ~140 min). The coefficients of variation are between 0.3 and 3.1%. **B.** FXm time-lapse
800 experiment using wild type cells in EMM at 32 °C without medium flow. **C.** FXm time-lapse
801 experiment using wild type cells in EMM at 32 °C with a constant flow of medium (3-5 $\mu L.min^{-1}$)
802 containing FITC-Dextran dye. *B*, *C*: individual traces represent the volume dynamics of single-cell
803 lineages (at each division, only one of the two daughter cells is further monitored). Volumes were
804 determined every 10 min. For display purposes, the individual traces are aligned to the first division
805 event (see Materials and Methods). Calculated average growth rates (with standard deviations) are
806 shown for each cycle. Note that the growth rate in the presence of a flow is consistent to that obtained
807 from the bulk analysis of a synchronized population (Fig. 4C).

808

809

810 **REFERENCES**

811 **Amodeo, A. A. and Skotheim, J. M.** (2016). Cell-Size Control. *Cold Spring Harb Perspect Biol* **8**,
812 a019083.

813 **Baybay, E. K., Esposito, E. and Hauf, S.** (2020). Pomegranate: 2D segmentation and 3D
814 reconstruction for fission yeast and other radially symmetric cells. *Scientific reports* **10**, 16580–
815 15.

816 **Beinhauer, J. D., Hagan, I. M., Hegemann, J. H. and Fleig, U.** (1997). Mal3, the fission yeast
817 homologue of the human APC-interacting protein EB-1 is required for microtubule integrity and
818 the maintenance of cell form. *The Journal of cell biology* **139**, 717–728.

819 **Bishop, A. C., Ubersax, J. A., Petsch, D. T., Matheos, D. P., Gray, N. S., Blethrow, J., Shimizu,**
820 **E., Tsien, J. Z., Schultz, P. G., Rose, M. D., et al.** (2000). A chemical switch for inhibitor-
821 sensitive alleles of any protein kinase. *Nature* **407**, 395–401.

822 **Bryan, A. K., Goranov, A., Amon, A. and Manalis, S. R.** (2010). Measurement of mass, density,
823 and volume during the cell cycle of yeast. *Proc. Natl. Acad. Sci. U.S.A.* **107**, 999–1004.

824 **Bryan, A. K., Hecht, V. C., Shen, W., Payer, K., Grover, W. H. and Manalis, S. R.** (2014).
825 Measuring single cell mass, volume, and density with dual suspended microchannel resonators.
826 *Lab Chip* **14**, 569–576.

827 **Cadart, C., Monnier, S., Grilli, J., Sáez, P. J., Srivastava, N., Attia, R., Terriac, E., Baum, B.,**
828 **Cosentino-Lagomarsino, M. and Piel, M.** (2018). Size control in mammalian cells involves
829 modulation of both growth rate and cell cycle duration. *Nat Commun* **9**, 3275–15.

830 **Cadart, C., Venkova, L., Recho, P., Lagomarsino, M. C. and Piel, M.** (2019). The physics of cell-
831 size regulation across timescales. *Nat. Phys.* **15**, 993–1004.

832 **Cadart, C., Zlotek-Zlotkiewicz, E., Venkova, L., Thouvenin, O., Racine, V., Le Berre, M.,**
833 **Monnier, S. and Piel, M.** (2017). Fluorescence eXclusion Measurement of volume in live cells.
834 *Methods Cell Biol.* **139**, 103–120.

835 **Chen, T., Gómez-Escoda, B., Munoz-Garcia, J., Babic, J., Griscom, L., Wu, P.-Y. J. and**
836 **Coudreuse, D.** (2016). A drug-compatible and temperature-controlled microfluidic device for
837 live-cell imaging. *Open Biol* **6**, 160156.

838 **Cook, M. and Tyers, M.** (2007). Size control goes global. *Curr. Opin. Biotechnol.* **18**, 341–350.

839 **Coudreuse, D. and Nurse, P.** (2010). Driving the cell cycle with a minimal CDK control network.
840 *Nature* **468**, 1074–1079.

841 **Das, M., Wiley, D. J., Medina, S., Vincent, H. A., Larrea, M., Oriolo, A. and Verde, F.** (2007).
842 Regulation of cell diameter, For3p localization, and cell symmetry by fission yeast Rho-GAP
843 Rga4p. *Molecular biology of the cell* **18**, 2090–2101.

844 **Facchetti, G., Knapp, B., Flor-Parra, I., Chang, F. and Howard, M.** (2019). Reprogramming
845 Cdr2-Dependent Geometry-Based Cell Size Control in Fission Yeast. *Current biology : CB* **29**,
846 350–358.e4.

847 **Fantes, P.** (1979). Epistatic gene interactions in the control of division in fission yeast. *Nature* **279**,
848 428–430.

849 **Fantes, P. A.** (1977). Control of cell size and cycle time in Schizosaccharomyces pombe. *J. Cell. Sci.*
850 **24**, 51–67.

851 **Fantes, P. A. and Nurse, P.** (1978). Control of the timing of cell division in fission yeast. Cell size
852 mutants reveal a second control pathway. *Experimental cell research* **115**, 317–329.

853 **Fantes, P. and Nurse, P.** (1977). Control of cell size at division in fission yeast by a growth-
854 modulated size control over nuclear division. *Experimental cell research* **107**, 377–386.

855 **Grant, N. A., Abdel Magid, A., Franklin, J., Dufour, Y. and Lenski, R. E.** (2021). Changes in Cell
856 Size and Shape during 50,000 Generations of Experimental Evolution with Escherichia coli.
857 *Journal of bacteriology* **203**.

858 **Hayles, J. and Nurse, P.** (1992). Genetics of the fission yeast Schizosaccharomyces pombe. *Annu.*
859 *Rev. Genet.* **26**, 373–402.

860 **Jeffares, D. C., Rallis, C., Rieux, A., Speed, D., Převorovský, M., Mourier, T., Marsellach, F. X.,**
861 **Iqbal, Z., Lau, W., Cheng, T. M. K., et al.** (2015). The genomic and phenotypic diversity of
862 Schizosaccharomyces pombe. *Nature genetics* **47**, 235–241.

863 **Jorgensen, P., Edgington, N. P., Schneider, B. L., Rupes, I., Tyers, M. and Futcher, B.** (2007).
864 The size of the nucleus increases as yeast cells grow. *Molecular biology of the cell* **18**, 3523–
865 3532.

866 **Lancaster, O. M., Le Berre, M., Dimitracopoulos, A., Bonazzi, D., Zlotek-Zlotkiewicz, E.,**
867 **Picone, R., Duke, T., Piel, M. and Baum, B.** (2013). Mitotic rounding alters cell geometry to
868 ensure efficient bipolar spindle formation. *Dev. Cell* **25**, 270–283.

869 **Lenski, R. E. and Travisano, M.** (1994). Dynamics of adaptation and diversification: a 10,000-
870 generation experiment with bacterial populations. *Proc. Natl. Acad. Sci. U.S.A.* **91**, 6808–6814.

871 **Li, Q., Rycaj, K., Chen, X. and Tang, D. G.** (2015). Cancer stem cells and cell size: A causal link?
872 *Semin. Cancer Biol.* **35**, 191–199.

873 **Lloyd, A. C.** (2013). The regulation of cell size. *Cell* **154**, 1194–1205.

874 **Marshall, W. F., Young, K. D., Swaffer, M., Wood, E., Nurse, P., Kimura, A., Frankel, J.,**
875 **Wallingford, J., Walbot, V., Qu, X., et al.** (2012). What determines cell size? *BMC Biol.* **10**,
876 101.

877 **Martin, S. G. and Berthelot-Grosjean, M.** (2009). Polar gradients of the DYRK-family kinase
878 Pom1 couple cell length with the cell cycle. *Nature* **459**, 852–856.

879 **Mata, J. and Nurse, P.** (1997). tea1 and the microtubular cytoskeleton are important for generating
880 global spatial order within the fission yeast cell. *Cell* **89**, 939–949.

881 **McDonald, J. C. and Whitesides, G. M.** (2002). Poly(dimethylsiloxane) as a material for fabricating
882 microfluidic devices. *Acc. Chem. Res.* **35**, 491–499.

883 **Millar, J. B., Buck, V. and Wilkinson, M. G.** (1995). Pyp1 and Pyp2 PTPases dephosphorylate an
884 osmosensing MAP kinase controlling cell size at division in fission yeast. *Genes & development*
885 **9**, 2117–2130.

886 **Mitchison, J. M.** (1957). The growth of single cells. I. Schizosaccharomyces pombe. *Experimental*
887 *cell research* **13**, 244–262.

888 **Mitchison, J. M. and Nurse, P.** (1985). Growth in cell length in the fission yeast
889 Schizosaccharomyces pombe. *J. Cell. Sci.* **75**, 357–376.

890 **Model, M.** (2020). Comparison of cell volume measurements by fluorescence and absorption
891 exclusion microscopy. *J Microsc* **280**, 12–18.

892 **Model, M. A.** (2018). Methods for cell volume measurement. *Cytometry A* **93**, 281–296.

893 **Mongold, J. A. and Lenski, R. E.** (1996). Experimental rejection of a nonadaptive explanation for
894 increased cell size in Escherichia coli. *Journal of bacteriology* **178**, 5333–5334.

895 **Moreno, S., Klar, A. and Nurse, P.** (1991). Molecular genetic analysis of fission yeast
896 Schizosaccharomyces pombe. *Meth. Enzymol.* **194**, 795–823.

897 **Moseley, J. B., Mayeux, A., Paoletti, A. and Nurse, P.** (2009). A spatial gradient coordinates cell
898 size and mitotic entry in fission yeast. *Nature* **459**, 857–860.

899 **Mueller, R. L.** (2015). Genome Biology and the Evolution of Cell-Size Diversity. *Cold Spring Harb*
900 *Perspect Biol* **7**, a019125.

901 **Navarro, F. J. and Nurse, P.** (2012). A systematic screen reveals new elements acting at the G2/M
902 cell cycle control. *Genome Biol.* **13**, R36.

903 **Neufeld, T. P., la Cruz, de, A. F., Johnston, L. A. and Edgar, B. A.** (1998). Coordination of growth
904 and cell division in the Drosophila wing. *Cell* **93**, 1183–1193.

905 **Neumann, F. R. and Nurse, P.** (2007). Nuclear size control in fission yeast. *The Journal of cell*
906 *biology* **179**, 593–600.

907 **Nurse, P.** (1975). Genetic control of cell size at cell division in yeast. *Nature* **256**, 547–551.

908 **Pan, K. Z., Saunders, T. E., Flor-Parra, I., Howard, M. and Chang, F.** (2014a). Cortical
909 regulation of cell size by a sizer cdr2p. *Elife* **3**, e02040.

910 **Pan, K. Z., Saunders, T. E., Flor-Parra, I., Howard, M. and Chang, F.** (2014b). Cortical
911 regulation of cell size by a sizer cdr2p. *Elife* **3**, e02040.

912 **Pedersen, S. F., Hoffmann, E. K. and Mills, J. W.** (2001). The cytoskeleton and cell volume
913 regulation. *Comp. Biochem. Physiol., Part A Mol. Integr. Physiol.* **130**, 385–399.

914 **Petersen, J.** (2009). TOR signalling regulates mitotic commitment through stress-activated MAPK
915 and Polo kinase in response to nutrient stress. *Biochem. Soc. Trans.* **37**, 273–277.

916 **Pietras, A.** (2011). Cancer stem cells in tumor heterogeneity. *Adv. Cancer Res.* **112**, 255–281.

917 **Revilla-Guarinos, M. T., Martín-García, R., Villar-Tajadura, M. A., Estravís, M., Coll, P. M.**
918 **and Pérez, P.** (2016). Rga6 is a Fission Yeast Rho GAP Involved in Cdc42 Regulation of
919 Polarized Growth. *Molecular biology of the cell*.

920 **Saunders, T. E., Pan, K. Z., Angel, A., Guan, Y., Shah, J. V., Howard, M. and Chang, F.** (2012).
921 Noise reduction in the intracellular pom1p gradient by a dynamic clustering mechanism. *Dev.*
922 *Cell* **22**, 558–572.

923 **Scheffler, K., Recouvreux, P., Paoletti, A. and Tran, P. T.** (2014). Oscillatory AAA+ ATPase
924 Knk1 constitutes a novel morphogenetic pathway in fission yeast. *Proc. Natl. Acad. Sci. U.S.A.*
925 **111**, 17899–17904.

926 **Soifer, I., Robert, L. and Amir, A.** (2016). Single-Cell Analysis of Growth in Budding Yeast and
927 Bacteria Reveals a Common Size Regulation Strategy. *Current biology : CB* **26**, 356–361.

928 **Soto, T., Villar-Tajadura, M. A., Madrid, M., Vicente, J., Gacto, M., Pérez, P. and Cansado, J.**
929 (2010). Rga4 modulates the activity of the fission yeast cell integrity MAPK pathway by acting
930 as a Rho2 GTPase-activating protein. *The Journal of biological chemistry* **285**, 11516–11525.

931 **Su, T. T. and O'Farrell, P. H.** (1998). Size control: cell proliferation does not equal growth. *Current*
932 *biology : CB* **8**, R687–9.

933 **Sun, S. and Gresham, D.** (2021). Cellular quiescence in budding yeast. *Yeast* **38**, 12–29.

934 **Sveiczer, A., Novak, B. and Mitchison, J. M.** (1996). The size control of fission yeast revisited. *J.*
935 *Cell. Sci.* **109 (Pt 12)**, 2947–2957.

936 **Taheri-Araghi, S., Bradde, S., Sauls, J. T., Hill, N. S., Levin, P. A., Paulsson, J., Vergassola, M.**
937 **and Jun, S.** (2015). Cell-size control and homeostasis in bacteria. *Current biology : CB* **25**, 385–
938 391.

939 **Villar-Tajadura, M. A., Coll, P. M., Madrid, M., Cansado, J., Santos, B. and Pérez, P.** (2008).
940 Rga2 is a Rho2 GAP that regulates morphogenesis and cell integrity in S. pombe. *Mol.*
941 *Microbiol.* **70**, 867–881.

942 **Vjestica, A., Zhang, D., Liu, J. and Oliferenko, S.** (2013). Hsp70-Hsp40 chaperone complex
943 functions in controlling polarized growth by repressing Hsf1-driven heat stress-associated
944 transcription. *PLOS Genetics* **9**, e1003886.

945 **Watanabe, N., Ishihara, T. and Ohshima, Y.** (2007). Mutants carrying two sma mutations are super
946 small in the nematode C. elegans. *Genes to cells : devoted to molecular & cellular mechanisms*
947 **12**, 603–609.

948 **Weigmann, K., Cohen, S. M. and Lehner, C. F.** (1997). Cell cycle progression, growth and
949 patterning in imaginal discs despite inhibition of cell division after inactivation of Drosophila
950 Cdc2 kinase. *Development* **124**, 3555–3563.

951 **Yang, J., Dungrawala, H., Hua, H., Manukyan, A., Abraham, L., Lane, W., Mead, H., Wright,**
952 **J. and Schneider, B. L.** (2011). Cell size and growth rate are major determinants of replicative
953 lifespan. *Cell cycle* **10**, 144–155.

954 **Zegman, Y., Bonazzi, D. and Minc, N.** (2015). Measurement and manipulation of cell size
955 parameters in fission yeast. *Methods Cell Biol.* **125**, 423–436.

956 **Zhurinsky, J., Leonhard, K., Watt, S., Marguerat, S., Bähler, J. and Nurse, P.** (2010). A
957 coordinated global control over cellular transcription. *Current biology : CB* **20**, 2010–2015.

958 **Zlotek-Zlotkiewicz, E., Monnier, S., Cappello, G., Le Berre, M. and Piel, M.** (2015). Optical
959 volume and mass measurements show that mammalian cells swell during mitosis. *The Journal of*
960 *cell biology* **211**, 765–774.

961

FIGURE 1

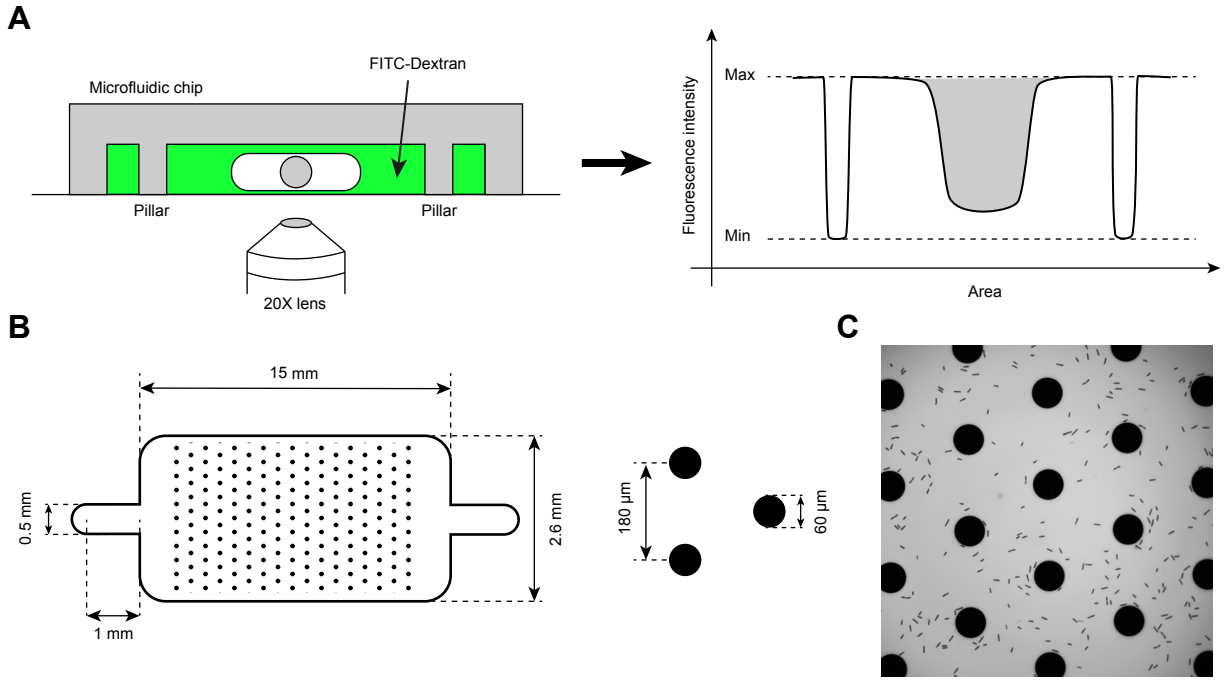
A
Microfluidic chip
FITC-Dextran
Pillar
Pillar
20X lens
Fluorescence intensity
Max
Min
Area
B
15 mm
0.5 mm
2.6 mm
1 mm
180 µm
60 µm
C

FIGURE 2

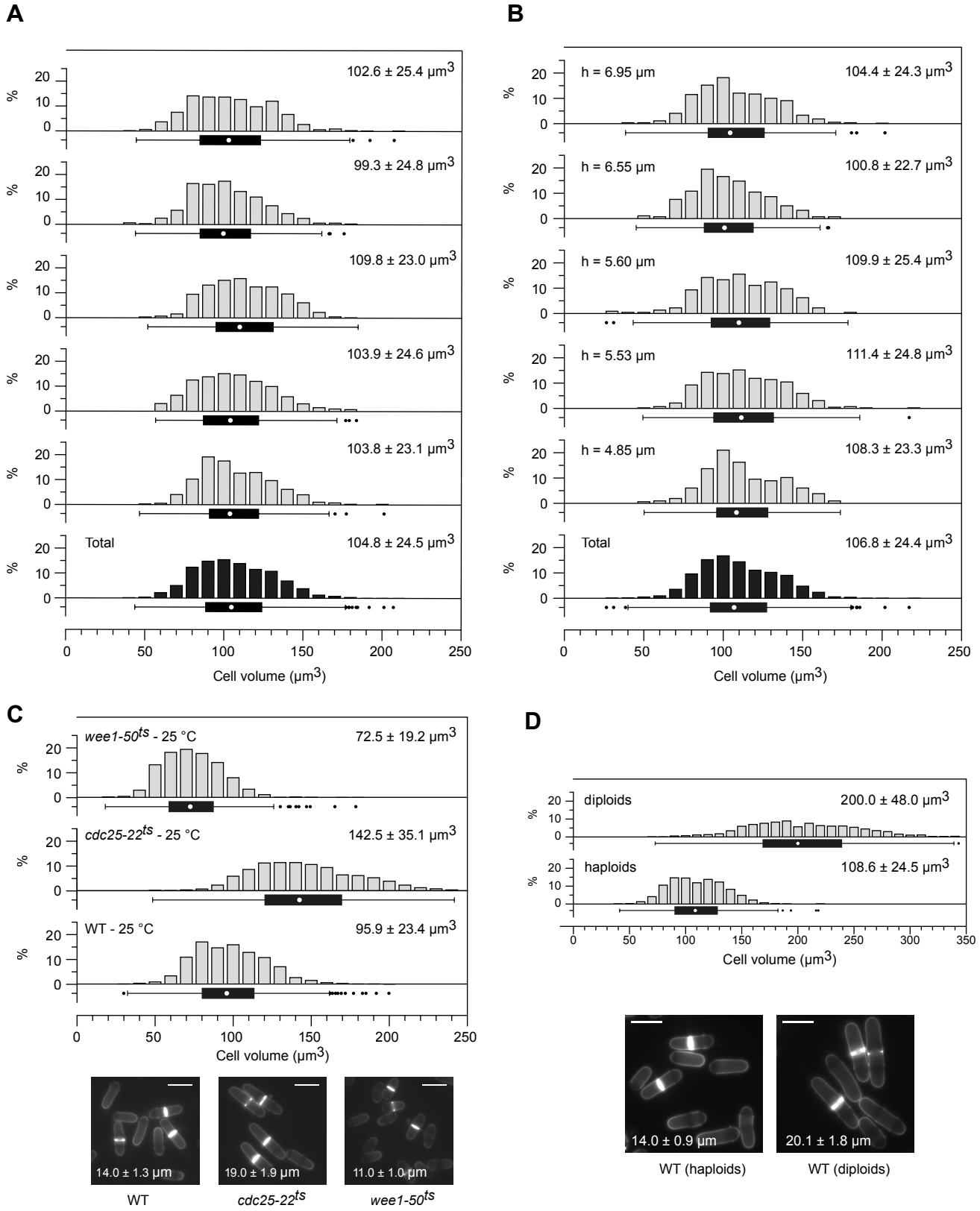
A
102.6 ± 25.4 μm3
99.3 ± 24.8 μm3
109.8 ± 23.0 μm3
103.9 ± 24.6 μm3
103.8 ± 23.1 μm3
Total
104.8 ± 24.5 μm3
Cell volume (μm3)
B
h = 6.95 μm
104.4 ± 24.3 μm3
h = 6.55 μm
100.8 ± 22.7 μm3
h = 5.60 μm
109.9 ± 25.4 μm3
h = 5.53 μm
111.4 ± 24.8 μm3
h = 4.85 μm
108.3 ± 23.3 μm3
Total
106.8 ± 24.4 μm3
Cell volume (μm3)
C
wee1-50ts - 25 °C
72.5 ± 19.2 μm3
cdc25-22ts - 25 °C
142.5 ± 35.1 μm3
WT - 25 °C
95.9 ± 23.4 μm3
Cell volume (μm3)
14.0 ± 1.3 μm
WT
19.0 ± 1.9 μm
cdc25-22ts
11.0 ± 1.0 μm
wee1-50ts
D
diploids
200.0 ± 48.0 μm3
haploids
108.6 ± 24.5 μm3
Cell volume (μm3)
14.0 ± 0.9 μm
WT (haploids)
20.1 ± 1.8 μm
WT (diploids)

FIGURE 3

A

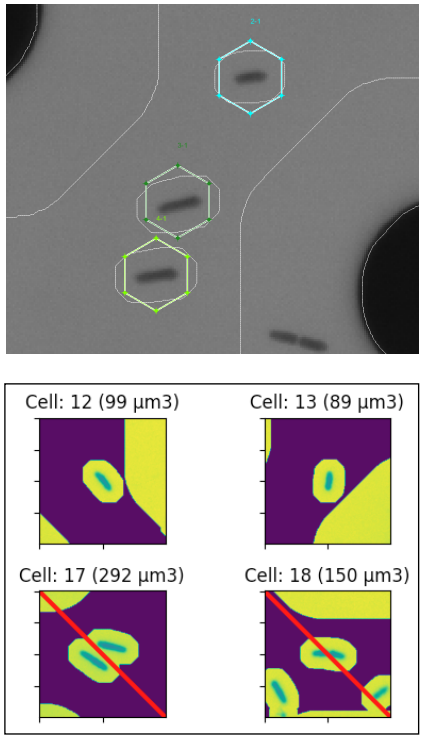
Cell: 12 (99 µm3)
Cell: 13 (89 µm3)
Cell: 17 (292 µm3)
Cell: 18 (150 µm3)

B

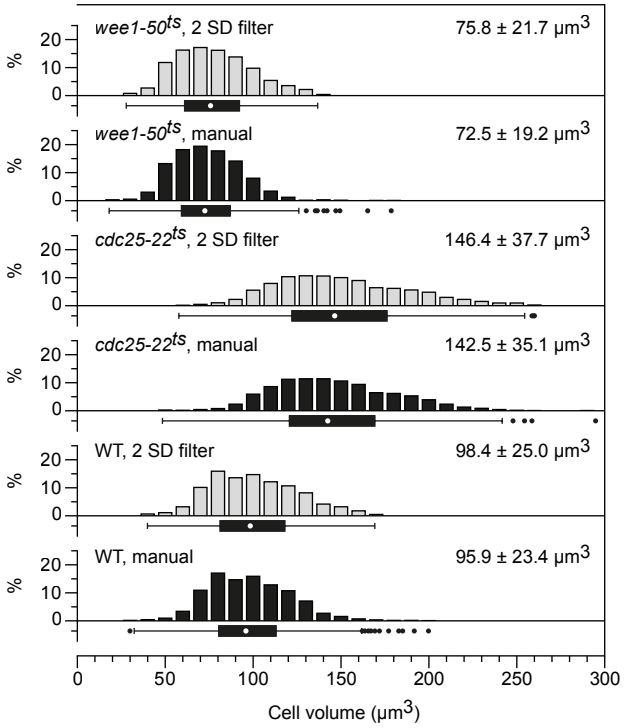
wee1-50ts, 2 SD filter
75.8 ± 21.7 µm3
wee1-50ts, manual
72.5 ± 19.2 µm3
cdc25-22ts, 2 SD filter
146.4 ± 37.7 µm3
cdc25-22ts, manual
142.5 ± 35.1 µm3
WT, 2 SD filter
98.4 ± 25.0 µm3
WT, manual
95.9 ± 23.4 µm3
%
0
10
20
0
50
100
150
200
250
300
Cell volume (µm3)

FIGURE 4

A

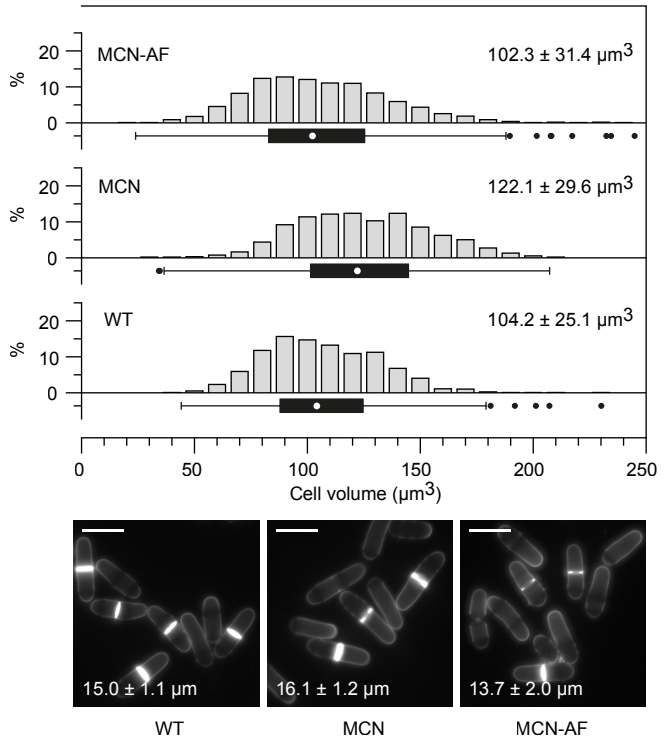

B

	25 °C	32 °C
	99.1 ± 21.8 µm^3	109.8 ± 23.0 µm^3
	97.8 ± 21.2 µm^3	103.9 ± 24.6 µm^3
	94.2 ± 20.4 µm^3	103.8 ± 23.1 µm^3
	93.6 ± 23.7 µm^3	102.6 ± 25.4 µm^3
	93.3 ± 20.5 µm^3	99.3 ± 24.8 µm^3
Full datasets:	**96.3 ± 21.9 µm^3**	**104.8 ± 24.5 µm^3**

C

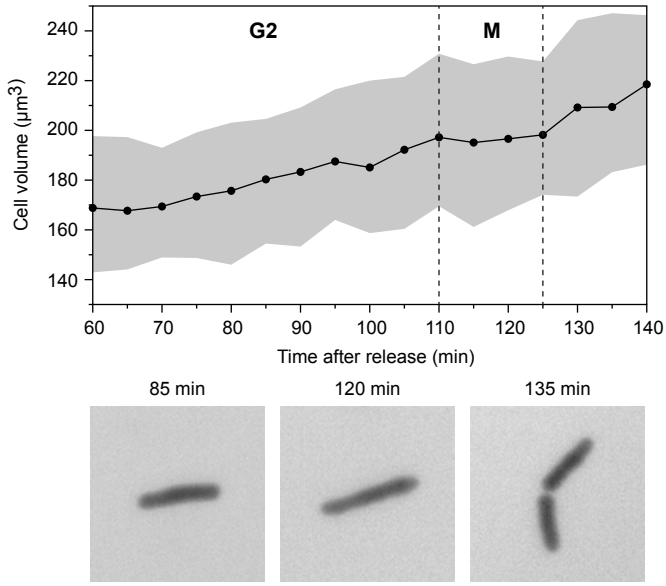

D

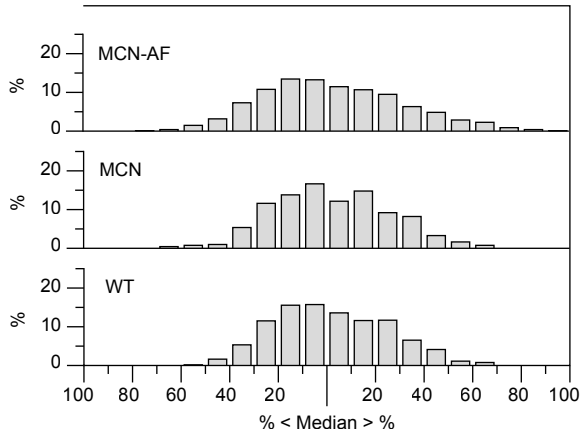

FIGURE 5

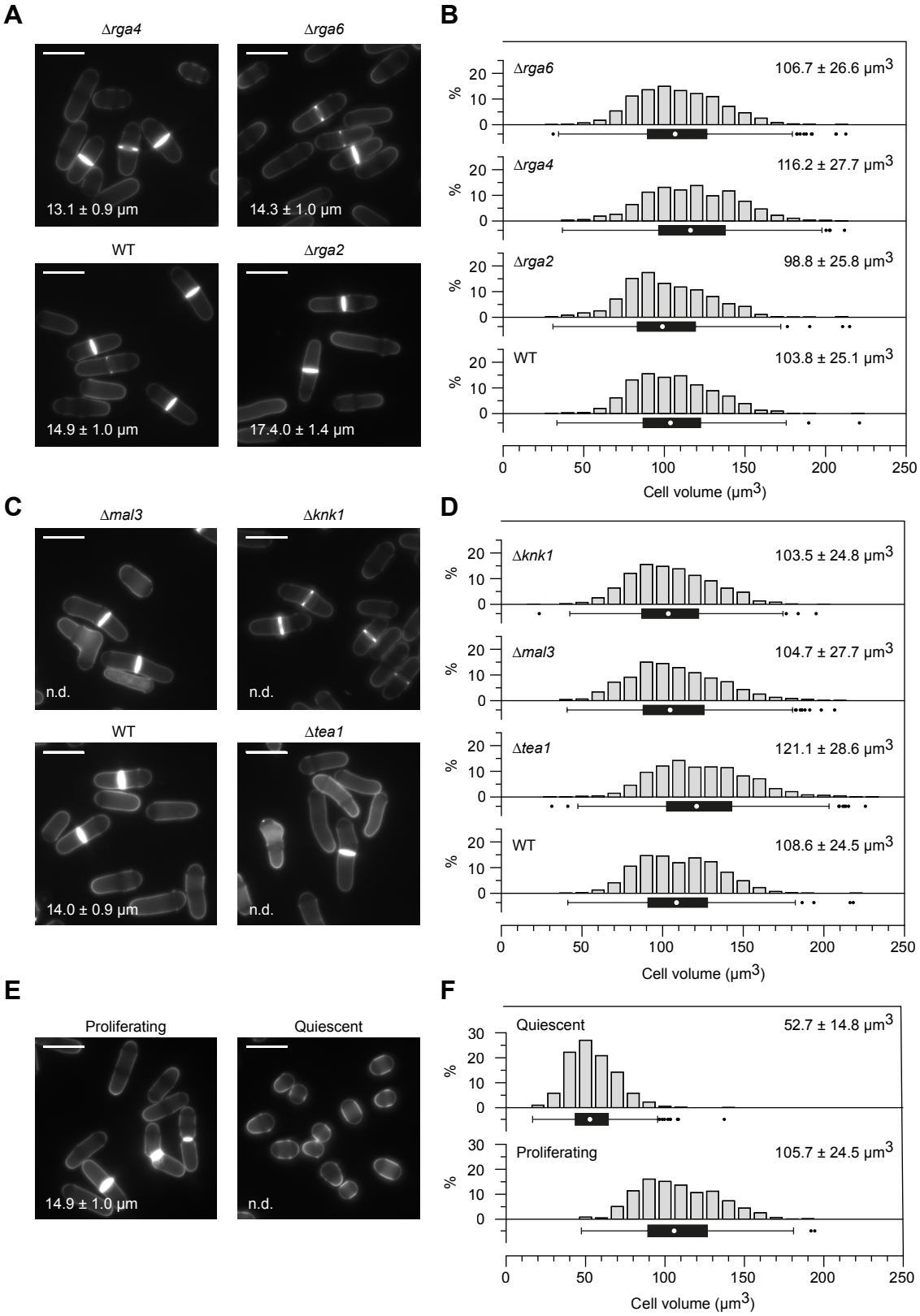
A
Δrga4
Δrga6
13.1 ± 0.9 µm
14.3 ± 1.0 µm
WT
Δrga2
14.9 ± 1.0 µm
17.4.0 ± 1.4 µm
B
Δrga6
106.7 ± 26.6 µm3
Δrga4
116.2 ± 27.7 µm3
Δrga2
98.8 ± 25.8 µm3
WT
103.8 ± 25.1 µm3
%
Cell volume (µm3)
C
Δmal3
Δknk1
n.d.
n.d.
WT
Δtea1
14.0 ± 0.9 µm
n.d.
D
Δknk1
103.5 ± 24.8 µm3
Δmal3
104.7 ± 27.7 µm3
Δtea1
121.1 ± 28.6 µm3
WT
108.6 ± 24.5 µm3
%
Cell volume (µm3)
E
Proliferating
Quiescent
14.9 ± 1.0 µm
n.d.
F
Quiescent
52.7 ± 14.8 µm3
Proliferating
105.7 ± 24.5 µm3
%
Cell volume (µm3)

FIGURE 6

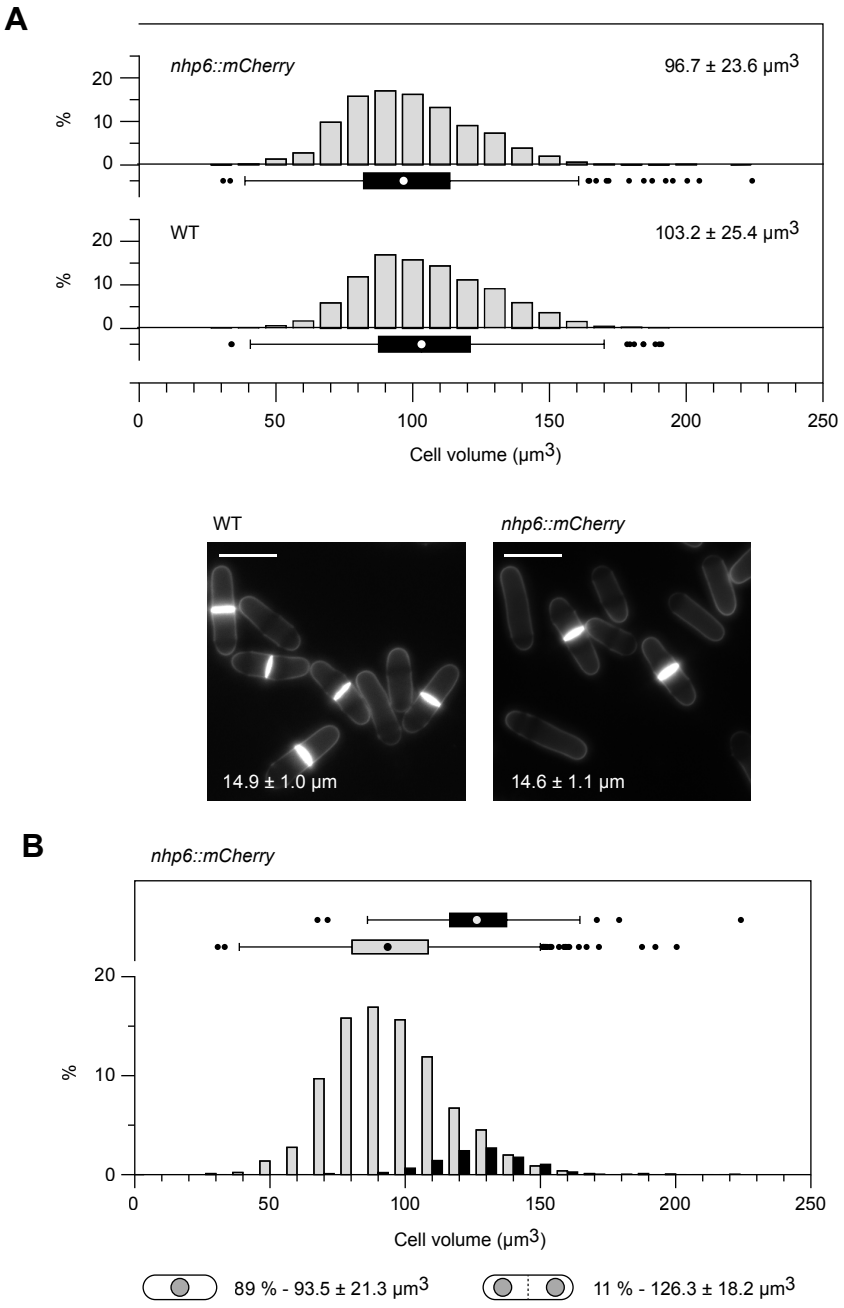
A
nhp6::mCherry
96.7 ± 23.6 µm3
WT
103.2 ± 25.4 µm3
%
20
10
0
0
50
100
150
200
250
Cell volume (µm3)
WT
nhp6::mCherry
14.9 ± 1.0 µm
14.6 ± 1.1 µm
B
nhp6::mCherry
89 % - 93.5 ± 21.3 µm3
11 % - 126.3 ± 18.2 µm3

FIGURE 7

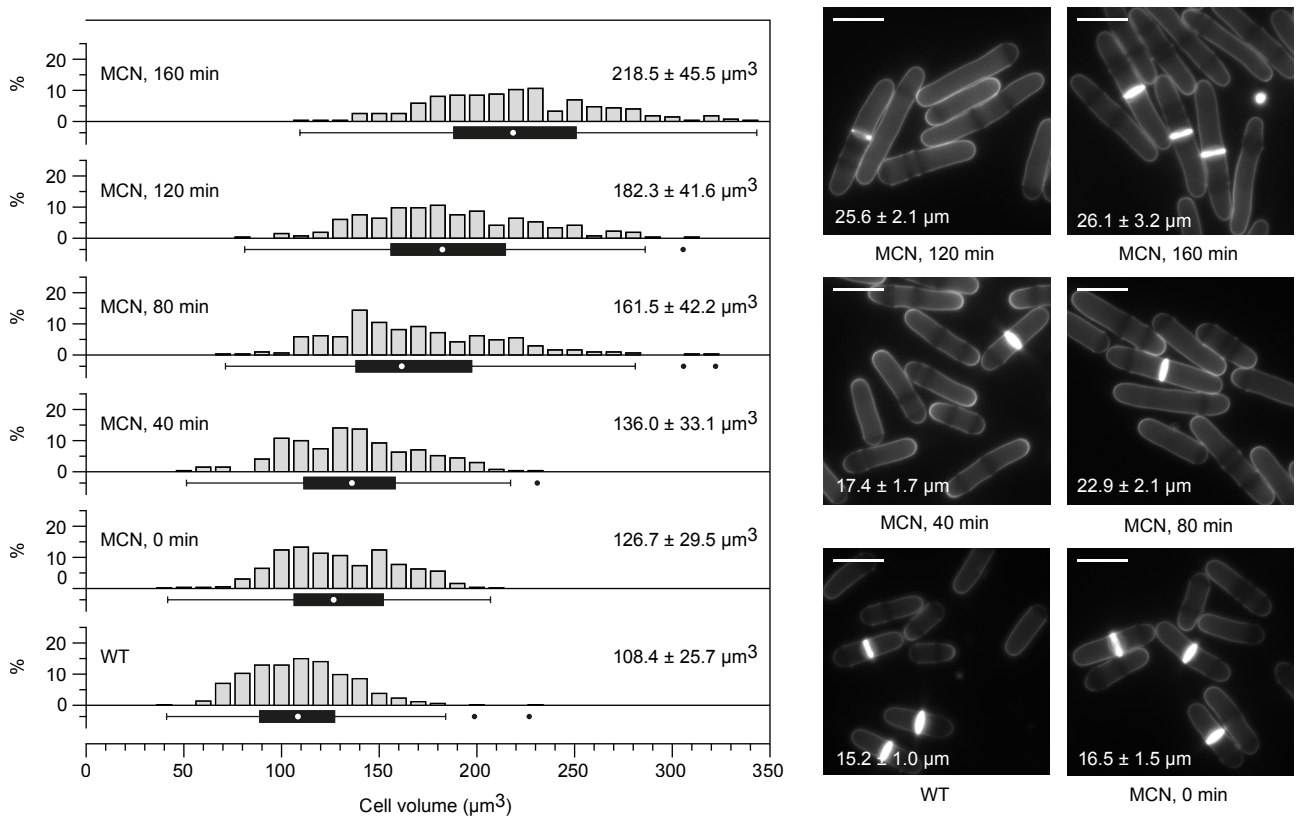
MCN, 160 min
218.5 ± 45.5 μm3
MCN, 120 min
182.3 ± 41.6 μm3
MCN, 80 min
161.5 ± 42.2 μm3
MCN, 40 min
136.0 ± 33.1 μm3
MCN, 0 min
126.7 ± 29.5 μm3
WT
108.4 ± 25.7 μm3
%
Cell volume (μm3)
25.6 ± 2.1 μm
MCN, 120 min
26.1 ± 3.2 μm
MCN, 160 min
17.4 ± 1.7 μm
MCN, 40 min
22.9 ± 2.1 μm
MCN, 80 min
15.2 ± 1.0 μm
WT
16.5 ± 1.5 μm
MCN, 0 min

FIGURE 8

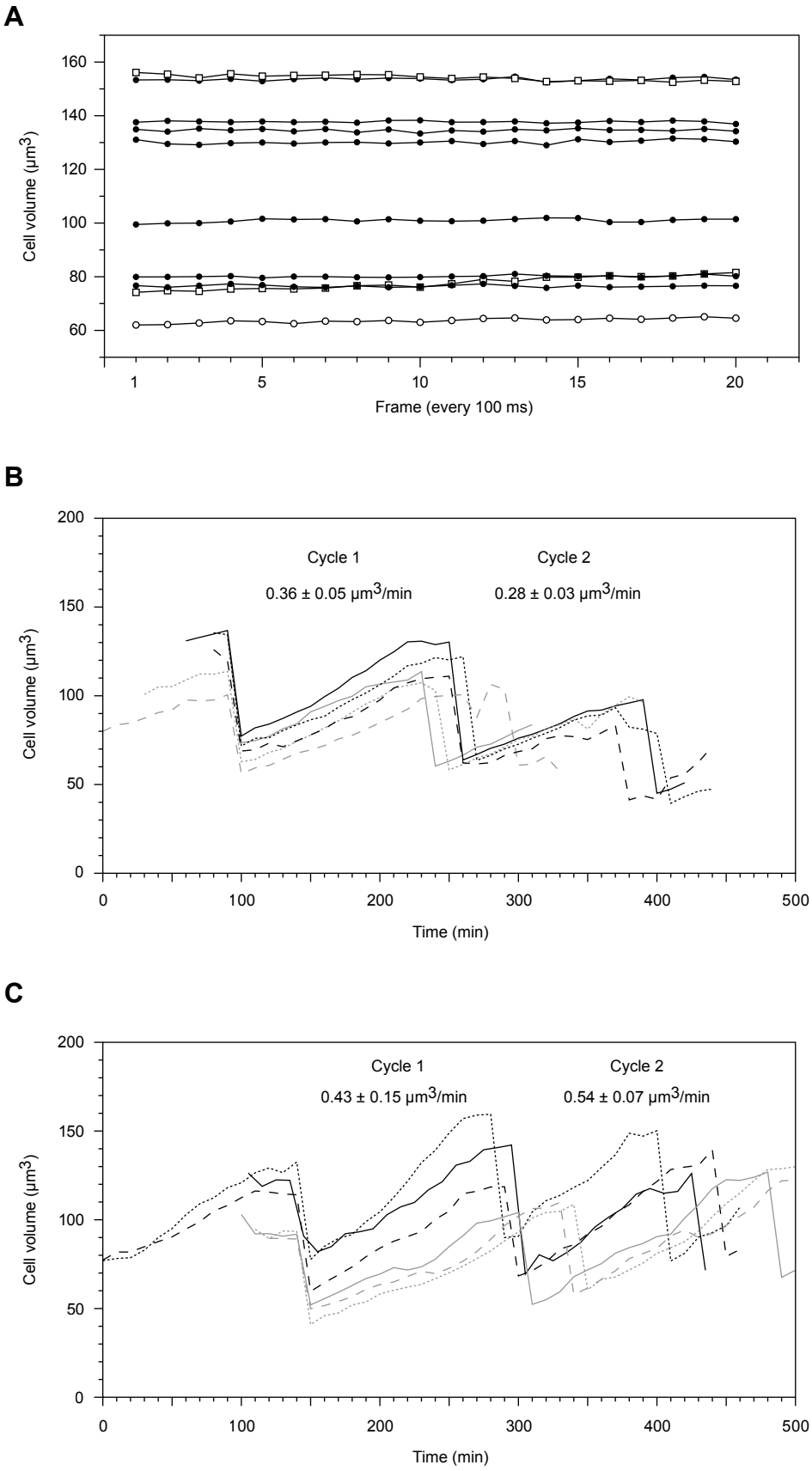
A
Cell volume (µm3)
160
140
120
100
80
60
1
5
10
15
20
Frame (every 100 ms)
B
Cell volume (µm3)
200
150
100
50
0
Cycle 1
0.36 ± 0.05 µm3/min
Cycle 2
0.28 ± 0.03 µm3/min
0
100
200
300
400
500
Time (min)
C
Cell volume (µm3)
200
150
100
50
0
Cycle 1
0.43 ± 0.15 µm3/min
Cycle 2
0.54 ± 0.07 µm3/min
0
100
200
300
400
500
Time (min)